iScience

CellPress
OPEN ACCESS

Article

CAR-T cells targeting HLA-G as potent therapeutic strategy for EGFR-mutated and overexpressed oral cancer

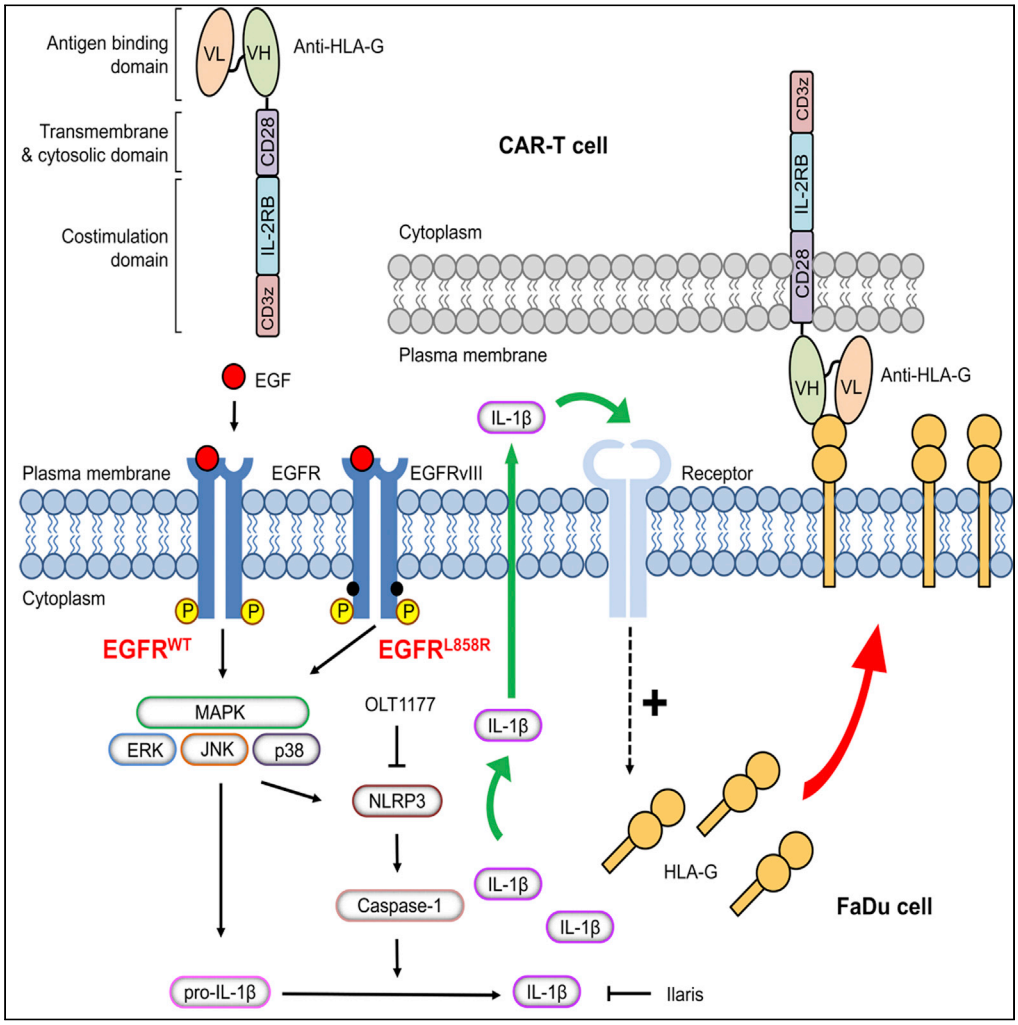

Yu-Chuan Lin, Chun-Hung Hua, Hsin-Man Lu, ..., Wei-Hua Huang, Der-Yang Cho, Chia-Ing Jan

janc1206@yahoo.com.tw

Highlights

To delineate the signal transduction of EGFR-NLRP3-HLA-G axis on OSCC

Aberrant EGFR confers OSCC on aggressive phenotype by regulating NLRP3 and HLA-G

Anti-HLA-G CAR-T cells protect against EGFR-overactive oral cancer

HLA-G targeting therapy provides an alternative strategy for OSCC treatment

Lin et al., iScience 26, 106089
March 17, 2023
https://doi.org/10.1016/j.isci.2023.106089

iScience

CellPress
OPEN ACCESS

Article

CAR-T cells targeting HLA-G as potent therapeutic strategy for EGFR-mutated and overexpressed oral cancer

Yu-Chuan Lin,[1,2,12] Chun-Hung Hua,[3,12] Hsin-Man Lu,[4,12] Shi-Wei Huang,[2,5] Yeh Chen,[5,6] Ming-Hsui Tsai,[3] Fang-Yu Lin,[2] Peter Canoll,[7] Shao-Chih Chiu,[1,2,6] Wei-Hua Huang,[8,9] Der-Yang Cho,[1,2,6,10] and Chia-Ing Jan[11,13,*]

SUMMARY

Oral squamous cell carcinoma (OSCC) is a common malignancy in the world. Recently, scientists have focused on therapeutic strategies to determine the regulation of tumors and design molecules for specific targets. Some studies have demonstrated the clinical significance of human leukocyte antigen G (HLA-G) in malignancy and NLR family pyrin domain-containing 3 (NLRP3) inflammasome in promoting tumorigenesis in OSCC. This is the first study to investigate whether aberrant epidermal growth factor receptor (EGFR) induces HLA-G expression through NLRP3 inflammasome-mediated IL-1β secretion in OSCC. Our results showed that the upregulation of NLRP3 inflammasome leads to abundant HLA-G in the cytoplasm and cell membrane of FaDu cells. In addition, we also generated anti-HLA-G chimeric antigen receptor (CAR)-T cells and provided evidence for their effects in EGFR-mutated and overexpressed oral cancer. Our results may be integrated with OSCC patient data to translate basic research into clinical significance and may lead to novel EGFR-aberrant OSCC treatment.

INTRODUCTION

Oral squamous cell carcinoma (OSCC) is the most frequent malignancy of the head and neck in the world.[1–3] Previous studies have shown that the survival rate is substantially reduced in patients with no effective treatment options.[4,5] Local infiltration and distant metastasis have been reported to be highly associated with mortality in patients with OSCC.[6,7] Moreover, rapid invasion and early lymph node metastasis with poor prognosis is correlated with an immunosuppressive tumor microenvironment that favors disease progression in OSCC.[8–10] However, the exact key molecules or signal transduction pathways involved in the deterioration of OSCC remain poorly understood.

Some reports have demonstrated that epidermal growth factor receptor (EGFR) is highly expressed in a variety of solid tumors.[11–13] The expression level of EGFR in OSCC tissues is higher than that in normal tissues and is correlated with tumor enlargement, advanced lymph node metastasis, and drug resistance.[14–16] Studies have also revealed that over 90% patients with OSCC expressed moderate to strong positive EGFR as evaluated by IHC staining.[17–19] Recently, targeting of EGFR has been utilized as a therapeutic strategy in clinical OSCC treatment for selected patients.[20,21] Unfortunately, few patients with OSCC with EGFR expression did not respond to EGFR inhibitors combined with tyrosine kinase inhibitor (TKI) therapy, which may be due to EGFR mutations.

Some studies have also demonstrated that EGFR mutations in patients with OSCC confer drug resistance and poor prognosis.[22,23] The most common EGFR mutations in head and neck squamous cell carcinoma are exon 19 deletion, L858R point mutation in exon 21, and in-frame deletion of EGFRvIII,[23,24] accounting for resistance to chemo and anti-EGFR therapies and enhanced tumor growth phenotype. Therefore, delineating the mechanism-promoting deterioration of OSCC and generating a novel therapeutic strategy for patients with advanced OSCC is urgently required.

Oral cancers are characterized by extensive immune cell infiltration, and cancer-related inflammation plays a critical role in OSCC carcinogenesis and tumor progression.[25–27] EGFR activation and signaling also play a potential role in NLR protein assembly, linked to inflammation.[28–30] Recently, inflammasome-mediated

[1]Drug Development Center, China Medical University, Taichung 404, Taiwan

[2]Translational Cell Therapy Center, China Medical University Hospital, No. 2, Yude Road, North District, Taichung 404, Taiwan

[3]Department of Otorhinolaryngology, China Medical University Hospital, Taichung 404, Taiwan

[4]Department of Psychology, Asia University, Taichung 404, Taiwan

[5]Institute of New Drug Development, China Medical University, Taichung 404, Taiwan

[6]Graduate Institute of Biomedical Sciences, China Medical University, Taichung 404, Taiwan

[7]Department of Pathology and Cell Biology, Columbia University, New York, NY 10032, USA

[8]Dr. Jean Landsborough Memorial Hospice Ward, Changhua Christian Hospital, Changhua 500, Taiwan

[9]Department of Nursing, Central Taiwan University of Science and Technology, Taichung 406, Taiwan

[10]Department of Neurosurgery, China Medical University Hospital, Taichung 404, Taiwan

[11]Department of Pathology and Laboratory Medicine, Kaohsiung Veterans General Hospital, Kaohsiung 813, Taiwan

[12]These authors contributed equally

[13]Lead contact

*Correspondence: janc1206@yahoo.com.tw

https://doi.org/10.1016/j.isci.2023.106089

cancer-related inflammation has been recognized in oncology, promoting tumor growth and metastasis. A subset of NLR proteins, NLRP3, controls inflammasome assembly, mediating the production of mature IL-1β and promoting malignant transformation of OSCC and aggressive tumor phenotypes.[31–33] In addition, MAPKs and NLRP3 inflammasome activation have been strongly implicated in the deterioration of OSCC in patients.[34,35] However, literature on the role of NLRP3 inflammasomes is still limited, and the regulation between EGFR variants and inflammasomes in cancer cells is lacking.

Recently, immune checkpoints are found as regulators of the immune system and considered novel targets for immunotherapy owing to their potential carcinogenic ability in solid tumors.[36–38] Human leukocyte antigen G (HLA-G), a non-classical HLA class I molecule of the human major histocompatibility complex, has been reported as an immune checkpoint molecule involved in the development of solid malignant neoplasms and inhibiting the cytolytic activity of cytotoxic T lymphocytes and NK cells.[39–42] The importance and advantage of investigating immune checkpoint molecules is that they are utilized in cancer immunotherapies with promising clinical outcomes for the treatment of OSCC.[43–45] However, the molecules involved in HLA-G production and the precise therapeutic effects of targeting HLA-G in OSCC are still to be identified.

In this study, we hypothesized that EGFR overexpression contributes to OSCC deterioration via MAPKs phosphorylation, NLRP3 inflammasome activation, and aberrant HLA-G expression. Targeting HLA-G may be beneficial in the treatment of OSCC. To the best of our knowledge, this is the first report to investigate the involvement of the EGFR-NLRP3 inflammasome-HLA-G axis in the development of OSCC. In addition, anti-HLA-G chimeric antigen receptor (CAR)-T cells, developed as a novel therapeutic strategy for EGFR mutants and TKI-resistant OSCC, will soon be applied to patients.

RESULTS

The expression of EGFR, EGFR^{L858R}, NLRP3, and HLA-G was increased and highly correlated with OSCC stage in human tissues

Although EGFR, NLRP3, and HLA-G are highly correlated with poor outcomes in patients with OSCC,[10,14,46] the correlation among these molecules is still absent. We recruited patients who were pathologically diagnosed with OSCC. Tumor tissues and paired normal adjacent noncancerous tissues (NAT) were collected; the NAT sample served as the control group. As shown in Figure 1A, total EGFR was highly expressed in the basement membrane and tumor invasive areas of OSCC tissues compared to those of control tissues, both in the early and late stages. In addition, EGFR^{L858R}, NLRP3, and HLA-G were slightly to moderately expressed in the early stage of OSCC, with strong staining in the late-stage OSCC tissue samples. The correlation of total EGFR, EGFR^{L858R}, and NLRP3 with HLA-G was evaluated. As shown in Figure 1B, EGFR expression in OSCC tissues was significantly positively correlated with HLA-G expression ($R = 0.7114$). In parallel, the expression of EGFR^{L858R} ($R = 0.6966$) or NLRP3 ($R = 0.6753$) in OSCC tissues was significantly positively correlated with HLA-G expression. To provide further evidence, the protein levels of total EGFR, phospho-EGFR (pEGFR), EGFR^{L858R}, NLRP3, and HLA-G were determined in tissue samples using Western blot analysis. As shown in Figure 1C, the protein levels of these molecules were significantly higher in the early stage of OSCC than in the NAT, and these effects were markedly increased in tissues from the late stage of OSCC. The presented data suggest that the expression of EGFR, pEGFR, EGFR^{L858R}, NLRP3, and HLA-G was highly correlated and involved in the deterioration of OSCC.

Cell viability, migration, invasion, and epithelial-mesenchymal transition were enhanced in EGFR variant overexpressing FaDu cells

To investigate the role of EGFR signaling in MAPKs, NLRP3, and HLA-G induction in OSCC, several stable EGFR variants overexpressing FaDu cells, including EGFR^{WT}, EGFR^{19del}, EGFR^{L858R}, and EGFR^{vIII}, were established. As shown in Figure 2A, Western blot analysis was performed to determine the expression of total EGFR, pEGFR, EGFR^{19del}, EGFR^{L858R}, and EGFR^{vIII} in these cells. The viability of these stable cells was analyzed using an MTT assay. It was demonstrated that the cell viability of EGFR variant overexpressing FaDu cells, including EGFR^{WT}, EGFR^{19del}, EGFR^{L858R}, and EGFR^{vIII}, had significantly increased compared to that of the control cells (Figure 2B). To further investigate the role of EGFR in epithelial-mesenchymal transition (EMT), E-cadherin and vimentin expression was determined in FaDu cells using western blotting. As shown in Figure 2C, the expression of E-cadherin was downregulated in FaDu cells overexpressing EGFR variants compared with that in control cells. Conversely, vimentin expression was upregulated in FaDu cells

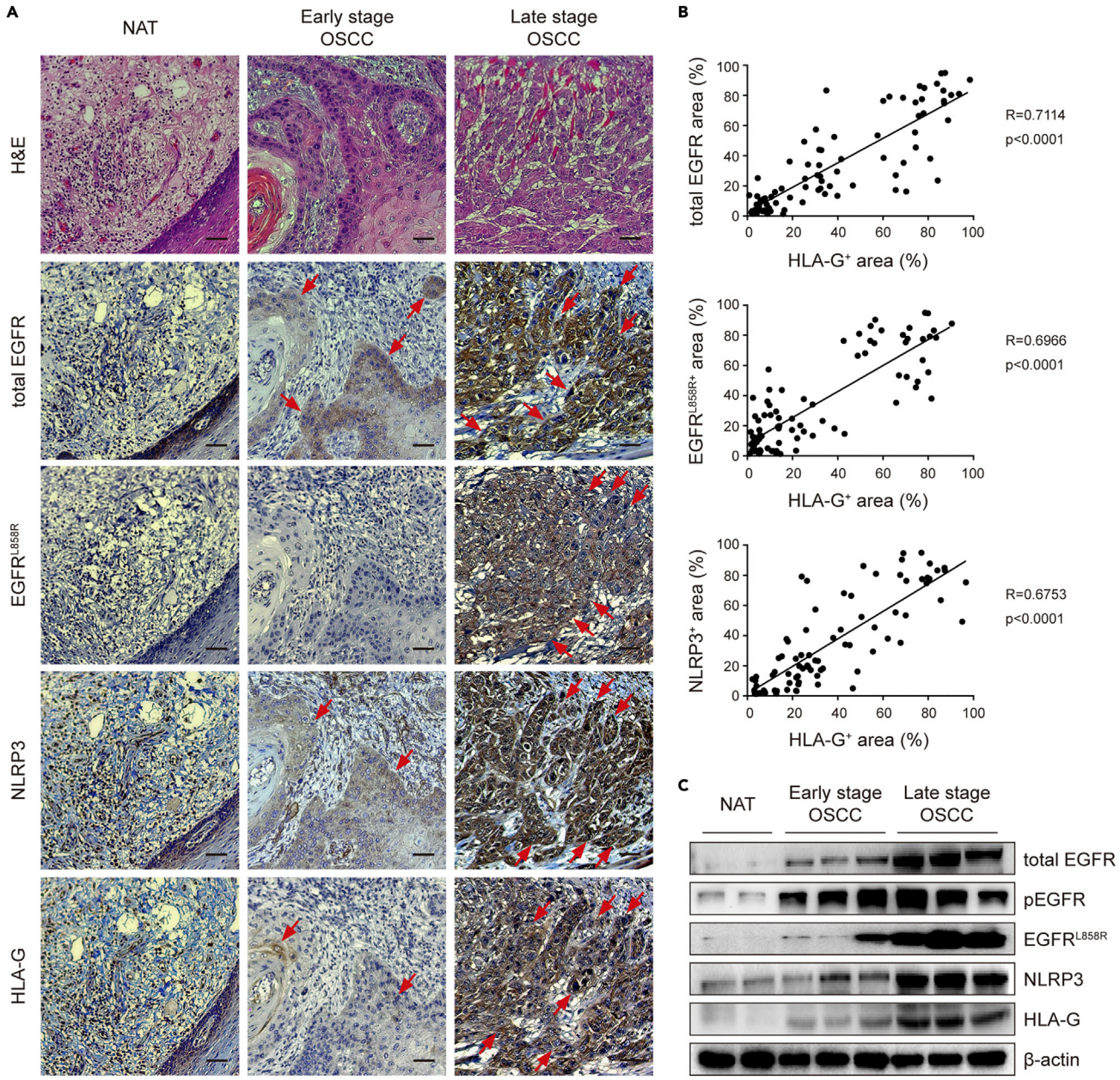

Figure 1. The expression of EGFR, EGFR^{L858R}, NLRP3, and HLA-G was increased and highly correlated with OSCC stage in human tissues

(A) H&E staining for paired normal adjacent noncancerous tissues (NAT), early stage, and late stage OSCC. The expression of total EGFR, EGFR^{L858R}, NLRP3, and HLA-G was analyzed by IHC staining. Red arrows indicated positive staining.

(B) R values between HLA-G and total EGFR, EGFR^{L858R}, or NLRP3.

(C) Representative Western blot analysis of the levels of total EGFR, pEGFR, EGFR^{L858R}, NLRP3, and HLA-G expression in human OSCC tissues. In A, the original magnification was x200. Scale bars, 50 μm.

overexpressing EGFR compared to that in control cells. In addition, the migration of these cells was determined using a scratch-wound assay and Transwell-based assay. As shown in Figures 2D and 2E, cell migration was markedly enhanced in FaDu cells overexpressing the EGFR variant compared to control cells. In parallel, a matrigel-coated Transwell-based invasion assay was performed. As shown in Figure 2F, the results demonstrated that the invasive ability of FaDu cells overexpressing the EGFR variant was notably increased compared with that of control cells. The presented data suggest that EGFR variant overexpression not only prolongs tumor survival but also induces EMT in FaDu cells.

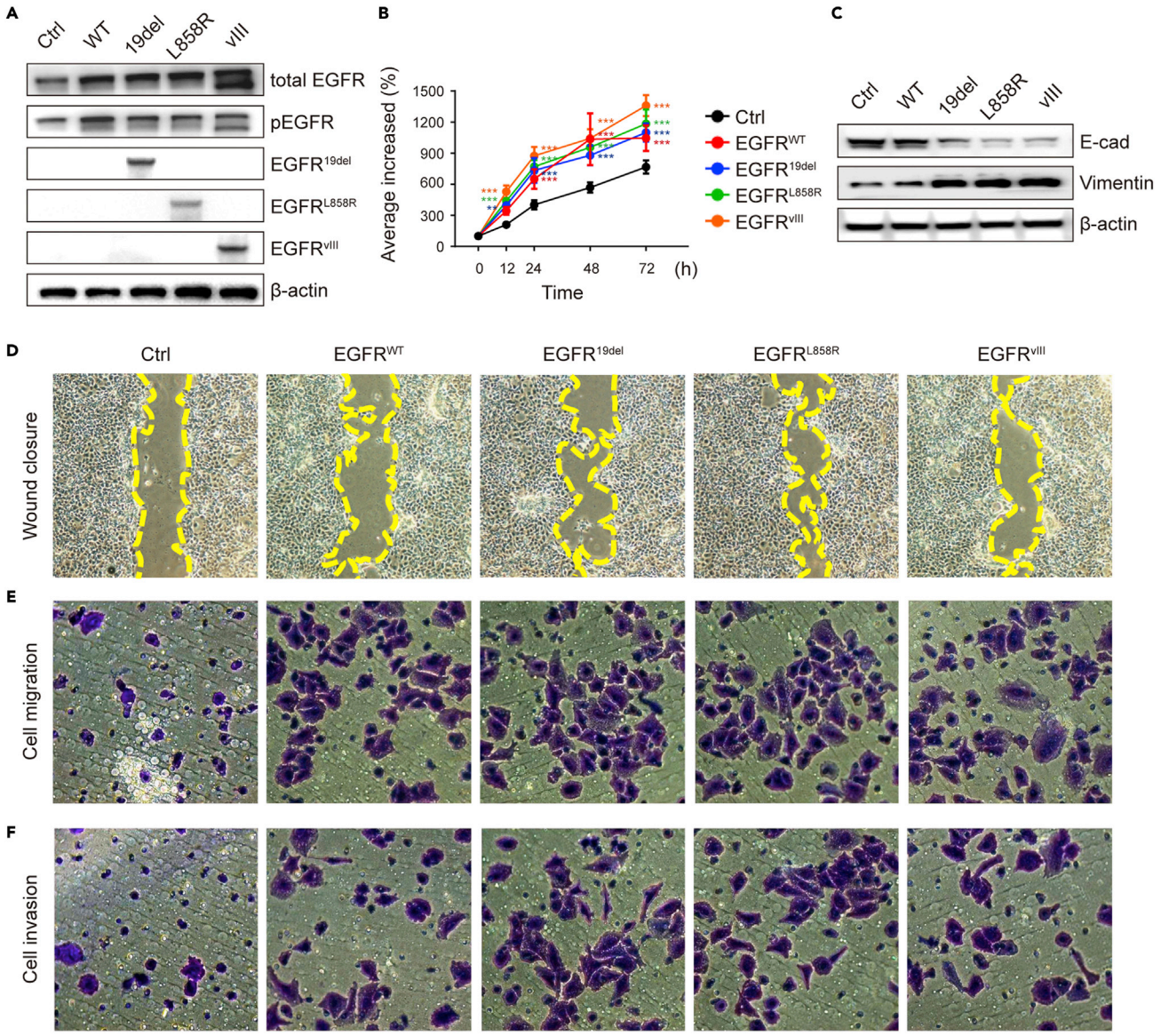

Figure 2. Cell viability, migration, invasion, and EMT were enhanced in EGFR variant overexpressing FaDu cells

(A) Establishment of EGFR variants expressing FaDu cells. Protein levels of total EGFR, pEGFR, EGFR^{19del}, EGFR^{L858R}, and EGFR^{vIII} were determined by Western blot analysis.

(B) Cell viability for control or EGFR variants expressing FaDu cells.

(C) Representative western blots showing levels of E-cadherin and vimentin in control or EGFR variants overexpressing FaDu cells.

(D) Wound healing, (E) cell migration, and (F) cell invasion assay was performed in control or EGFR variants overexpressing FaDu cells at indicated times. In B, data were expressed as mean ± SEM for six separate experiments. **$p < 0.01$, ***$p < 0.001$.

MAPKs phosphorylation, NLRP3 inflammasome activation, and HLA-G augmentation were enhanced in EGFR variant overexpressing FaDu cells

As shown in Figure 3A, the expression of pERK, pJNK, pp38, NLRP3, pro-IL-1β, and HLA-G was markedly upregulated in FaDu cells overexpressing the EGFR variant compared to control cells. Furthermore, the protein levels of mature IL-1β in EGFR variant overexpressing FaDu cell supernatants were significantly higher than those in control cells, as evaluated by ELISA (Figure 3B). These results suggest that EGFR variants positively regulate MAPKs phosphorylation, NLRP3 inflammasome activation, IL-1β secretion, and HLA-G augmentation, which may contribute to the deterioration of OSCC (Figure 3C).

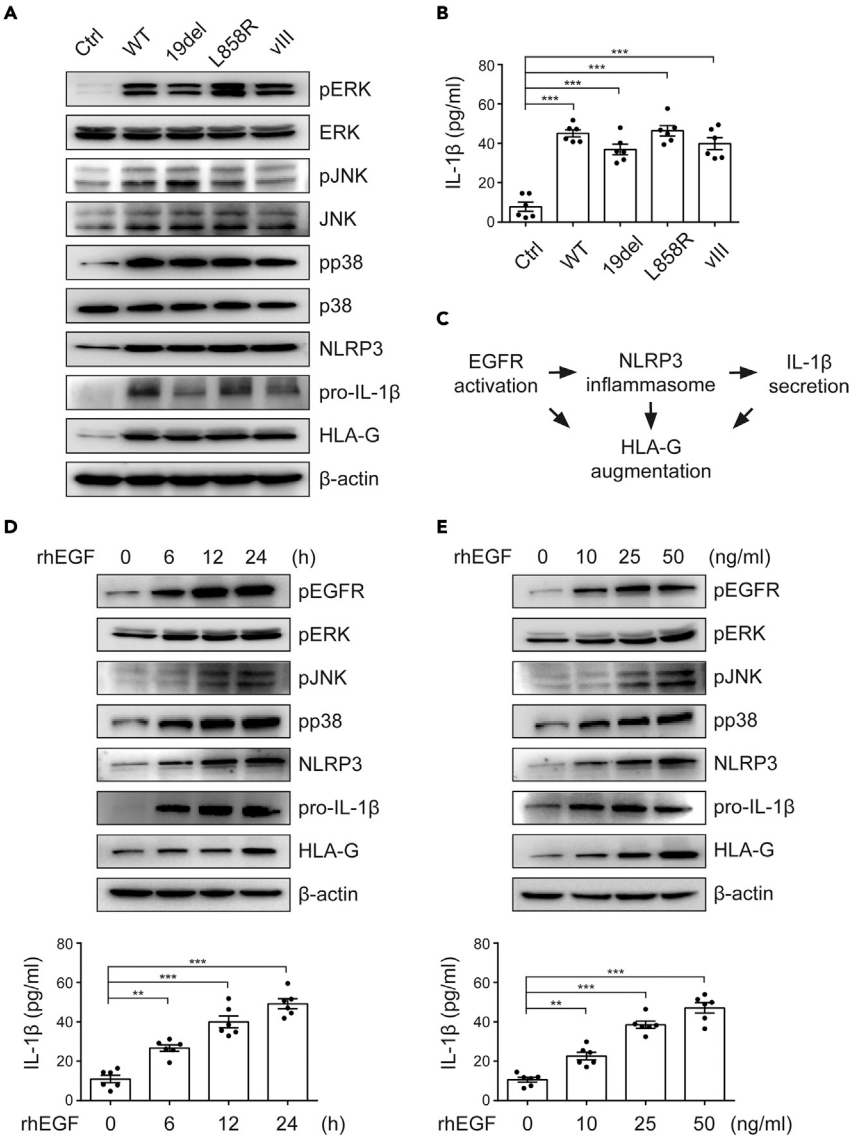

Figure 3. MAPKs phosphorylation, NLRP3 inflammasome activation, and HLA-G augmentation were enhanced in EGFR variant overexpressing FaDu cells

(A) Representative western blots showing levels of pERK, pJNK, pp38, NLRP3, pro-IL-1β, and HLA-G proteins in control or EGFR variants overexpressing FaDu cells.

(B) ELISA for protein levels of IL-1β in control or EGFR variants overexpressing FaDu cell supernatants.

(C) Proposed pathways indicated EGFR activation, NLRP3 inflammasome, IL-1β secretion, and HLA-G augmentation may contribute to the deterioration of OSCC.

(D) pEGFR, pERK, pJNK, pp38, NLRP3, pro-IL-1β, and HLA-G protein levels were determined by western blotting and matured IL-1β was detected by ELISA after incubated with rhEGF for 0, 6, 12, or 24 h in FaDu cells.

(E) pEGFR, pERK, pJNK, pp38, NLRP3, pro-IL-1β, and HLA-G protein levels were determined by western blotting and matured IL-1β was detected by ELISA after incubated with 0, 10, 25, or 50 ng/mL rhEGF for 24 h in FaDu cells. β-actin was used as an internal control. Data were mean ± SEM of six separate experiments. **p < 0.01, ***p < 0.001.

To investigate the signal transduction of EGFR, FaDu cells were incubated with or without recombinant human EGF (rhEGF). As shown in Figures 3D and 3E, pEGFR, pERK, pJNK, pp38, NLRP3, pro-IL-1β, and HLA-G were markedly upregulated by rhEGF in a time- and dose-dependent manner. In addition, the protein levels of mature IL-1β in rhEGF-treated FaDu cell supernatants were significantly higher than those in control cells in a time- and dose-dependent manner, as evaluated by ELISA. The protein levels of IL-18 in control or EGFR variant overexpressing FaDu cell supernatants were low, and there was no significant

difference among these groups. A similar phenotype was noted in rhEGF-treated FaDu cell supernatants (Figure S1).

EGFR signaling induced NLRP3 inflammasome activation and HLA-G augmentation via MAPKs in FaDu cells

The potential transduction pathways involved in the EGFR variants were further examined in cell models with selective inhibitors and specific short hairpin RNAs (shRNAs). Notably, MAPKs serve as potent activators of the priming signal of NLRP3 inflammasome.[35,47] In addition, various molecules and cytokines have been shown to increase the expression of HLA-G, which may be followed by NLRP3 inflammasome activation.

PD98059, an ERK inhibitor, was used to further confirm this observation. Cells were pretreated with DMSO or several doses of PD98059 for 1 h, followed by incubation with rhEGF. As shown in Figure 4A, the expression of NLRP3, pro-IL-1β, and HLA-G was downregulated by PD98059 under rhEGF treatment compared with that in rhEGF-treated cells. The protein levels of mature IL-1β in PD98059-treated FaDu cell supernatants were significantly downregulated compared to those in rhEGF-treated only cells, as evaluated by ELISA.

We then examined whether the upregulation of IL-1β and HLA-G was mediated by NLRP3 inflammasome activation and the effects of NLRP3 inflammasomes in the EMT of rhEGF-treated FaDu cells. OLT1177 was used as the NLRP3 inhibitor in this study. As shown in Figure 4B, the expression of pro-IL-1β was only slightly downregulated by OLT1177 under rhEGF treatment compared to that in rhEGF-treated cells. In parallel, the protein levels of HLA-G and vimentin were markedly decreased by OLT1177 in rhEGF-treated cells compared with rhEGF-treated cells. E-cadherin was upregulated by OLT1177 under rhEGF treatment compared to that in rhEGF-treated cells. Notably, although the expression of pro-IL-1β was only slightly decreased during OLT1177 treatment, the protein levels of mature IL-1β in cell supernatants were significantly downregulated by OLT1177 compared to the rhEGF only group. Similarly, the IL-1 targeting monoclonal antibody, Ilaris, was used to investigate the role of IL-1 in HLA-G expression and EMT during rhEGF treatment. As shown in Figure 4C, the expression of pro-IL-1β, HLA-G, and vimentin was significantly downregulated, whereas E-cadherin was upregulated by Ilaris under rhEGF treatment compared with rhEGF-treated cells. In addition, the protein levels of mature IL-1β in cell supernatants were significantly downregulated by Ilaris compared with the rhEGF only group.

To further clarify the signal transduction of EGFR, NLRP3, and HLA-G, shRNAs were used to silence the gene expression. As shown in Figure 4D, rhEGF only slightly elevated the protein levels of pEGFR, NLRP3, pro-IL-1β, and HLA-G in the shEGFR group compared to the control FaDu cells treated with rhEGF. The effect of shEGFR on mature IL-1β secretion was confirmed by measuring the expression levels of IL-1β in the supernatants using ELISA. Meanwhile, rhEGF did not influence the expression level of pEGFR in the shNLRP3 group compared to that in the control FaDu cells treated with rhEGF (Figure 4E). However, shNLRP3 strongly prevented the expression of NLRP3, pro-IL-1β, and HLA-G compared to control FaDu cells treated with rhEGF. The effect of shNLRP3 on mature IL-1β was confirmed by measuring the expression levels of IL-1β in the supernatants using ELISA. Moreover, while shHLA-G significantly abolished the expression of HLA-G in rhEGF-treated shHLA-G FaDu cells, the protein levels of pEGFR, NLRP3, and pro-IL-1β did not change (Figure 4F). The effect of shHLA-G on mature IL-1β was confirmed by measuring the expression levels of IL-1β in the supernatants using ELISA. These results suggest that EGFR signaling induces EMT in FaDu cells by enhancing MAPKs phosphorylation, NLRP3 inflammasome activation, and HLA-G augmentation.

IL-1β induced HLA-G augmentation on cell membrane of FaDu cells that facilitated the cell killing ability of anti-HLA-G CAR-T cells

Inflammation has been shown to play a key role in OSCC processes.[6] NLPR3 and IL-1β inhibitors are widely used in clinical settings. However, the safety and side effects of using these reagents or antibodies remains a concern.[48,49] Recently, targeting tumor-associated antigens has been suggested as a powerful strategy for cancer therapy with fewer adverse reactions.[41,42] Based on the results above, HLA-G was not only upregulated in human OSCC but also in $EGFR^{WT}$, $EGFR^{19del}$, $EGFR^{L858R}$, and $EGFR^{vIII}$ and transformed stable FaDu cells. Therefore, we performed additional *in vitro* studies to evaluate the feasibility of the anti-HLA-G-based immune therapy. As shown in Figure 5A, HLA-G was not only upregulated in the cytoplasm but also expressed on the cell surface of FaDu cells overexpressing EGFR variants compared to control cells. To

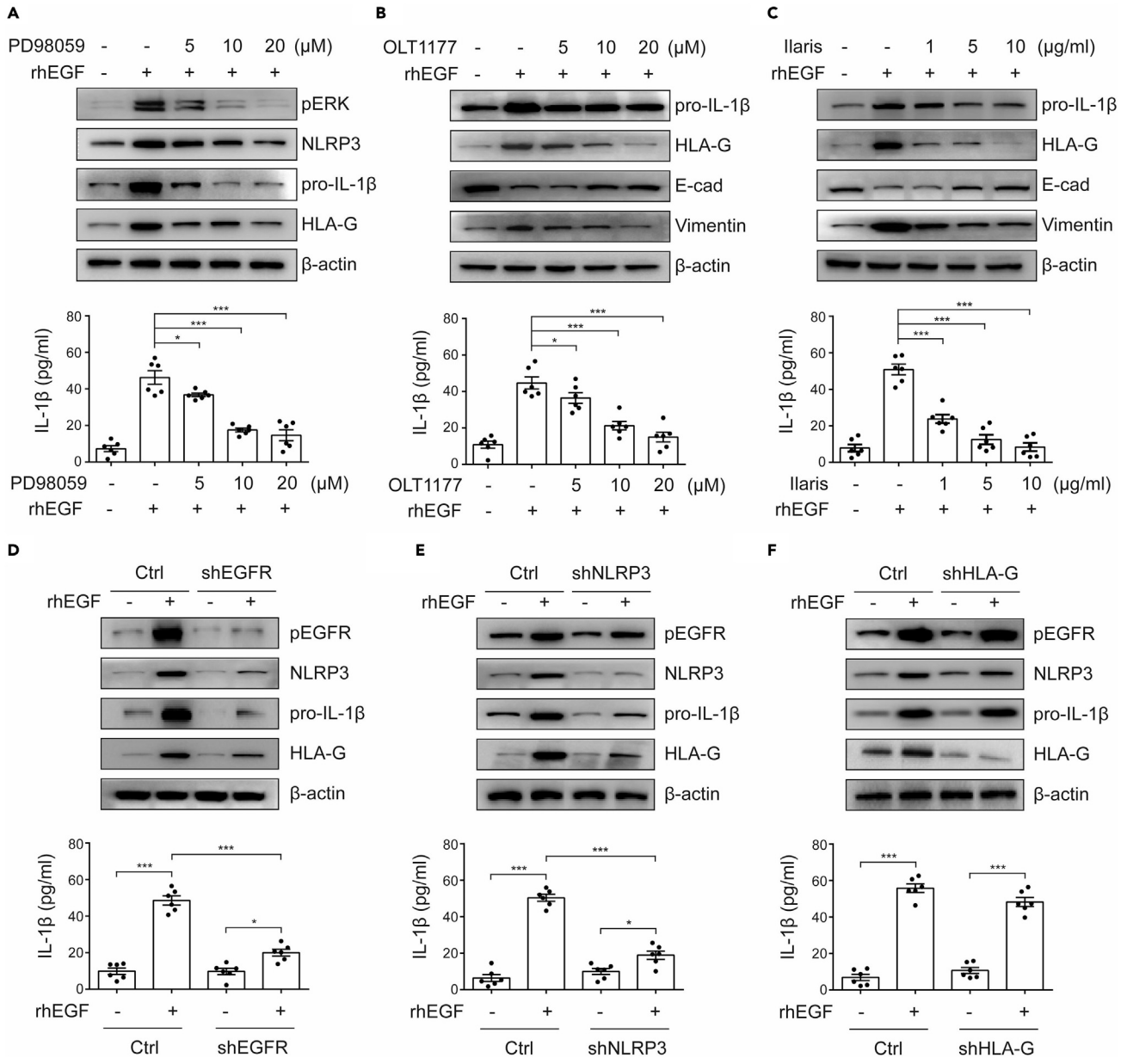

Figure 4. EGFR signaling induced NLRP3 inflammasome activation and HLA-G augmentation via MAPKs in FaDu cells

Cells were incubated with (A) ERK inhibitor, PD98059; NLRP3, pro-IL-1β, and HLA-G protein levels were determined by western blot and matured IL-1β was detected by ELISA. Cells were incubated with (B) NLRP3 inflammasome inhibitor, OLT1177, or (C) IL-1 inhibitor, Ilaris; pro-IL-1β, HLA-G, E-cadherin, and vimentin protein levels were measured by western blot and matured IL-1β was detected by ELISA. pEGFR, NLRP3, pro-IL-1β, and HLA-G protein levels by western blotting and matured IL-1β was detected by ELISA after incubated with or without rhEGF in control and (D) shEGFR, (E) shNLRP3, or (F) shHLA-G FaDu cells. β-actin was used as an internal control. Data were mean ± SEM of six separate experiments. *$p < 0.05$, ***$p < 0.001$.

investigate whether IL-1β could directly induce HLA-G production, cells were incubated with recombinant human IL-1β (rhIL-1β). As shown in Figures 5B and 5C, HLA-G expression was significantly enhanced by rhIL-1β stimulation in a time- and dose-dependent manner, as observed by western blotting and flow cytometry.

To target HLA-G, an anti-HLA-G single-chain variable fragment (scFv) containing CD28 domain, IL-2RB domain, and CD3 zeta domain expressing plasmid was constructed and prepared for T cell transduction. The transduction efficiency was approximately 36.6%, as examined by protein-L staining (Figure 5D). The transduced T cell population was determined by flow cytometry. As shown in Figure 5E, there were

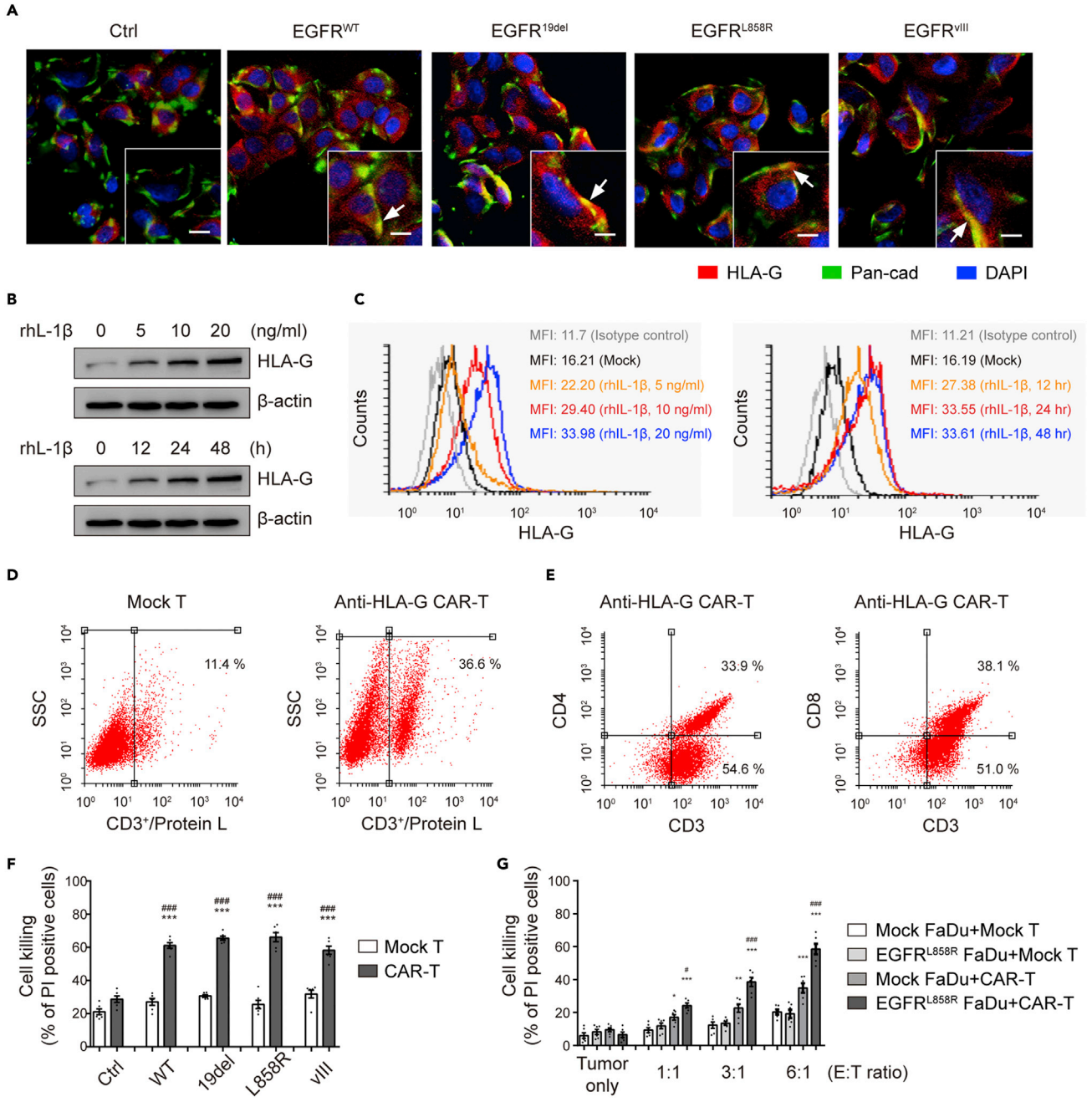

Figure 5. IL-1β induced HLA-G augmentation of the cell membrane of FaDu cells, which facilitated the cell killing ability of anti-HLA-G CAR-T cells

(A) HLA-G expression in FaDu cells overexpressing EGFR variants was determined by immunofluorescence.

(B) Total HLA-G protein levels were evaluated by western blotting, or (C) membrane HLA-G was analyzed by flow cytometry after incubated with 0, 5, 10, or 20 ng/mL rhIL-1β for 0, 12, 24, or 48 h in FaDu cells. Flow cytometric data were shown as histogram overlays.

(D) Analysis of transduction efficiency of the anti-HLA-G CAR plasmid on primary T cells. Transduction efficiency was evaluated by flow cytometry using fluorescent-tagged protein L to detect variable light chain Ig, together with human HLA-G protein.

(E) Anti-HLA-G CAR-T cell population analyzed using CD3 with CD4 or CD8 by flow cytometry.

(F) Cell killing ability of mock T cells and anti-HLA-G CAR-T cells in FaDu cells overexpressing EGFR variants.

(G) Cell killing ability of anti-HLA-G CAR-T cells on $EGFR^{L858R}$-overexpressing FaDu cells; E:T ratios of 1:1, 3:1, and 6:1. β-actin was used as an internal control. Data are expressed as the mean ± SEM of six separate experiments. Scale bars, 20 μm. White arrows indicated positive staining of HLA-G on the cell membrane. *p < 0.05, **p < 0.01, ***p < 0.001 compared to their mock T cells-treated group. #p < 0.05, ###p < 0.001 compared to mock FaDu cells treated with CAR-T cells.

approximately 33.9% $CD4^+/CD3^+$ cells and 38.1% $CD8^+/CD3^+$ cells after T cell expansion. To elucidate which type of HLA-G isoform could be recognized by our anti-HLA-G CAR-T cells, cell-based ELISA was performed. As shown in Figure S2, our anti-HLA-G CAT-T cells could bind to HLA-G1, -G2, -G4, -G5, and -G6 but not with HLA-G3 and -G7 isoforms. The specificity of anti-HLA-G CAR-T cells was also evaluated, and the results are shown in Figure S3.

The mock or anti-HLA-G plasmid-transduced T cells were then co-cultured with mock or EGFR variant-expressing FaDu cells. Next, cell killing ability was analyzed by propidium iodide (PI) staining. As shown in Figure 5F, cell killing ability was significantly increased in $EGFR^{WT}$-, $EGFR^{19del}$-, $EGFR^{L858R}$-, and EGFRvIII-expressing FaDu cells co-cultured with anti-HLA-G CAR-T cells compared with mock FaDu cells co-cultured with anti-HLA-G CAR-T cells. Furthermore, cell killing ability analysis was performed by PI staining with effector/target (E/T) ratios of 1:1, 3:1, or 6:1 in control or $EGFR^{L858R}$ FaDu cells. As shown in Figure 5G, the cell killing ability was significantly increased in $EGFR^{L858R}$-expressing FaDu cells co-cultured with anti-HLA-G CAR-T cells and was positively correlated with the E/T ratio. These results suggest that IL-1β induces HLA-G augmentation on the cell membrane, which could be an ideal target for CAR-T-based cell therapy.

Anti-HLA-G CAR-T cell therapy effectively decreased tumor growth and metastasis in EGFR variants overexpressing FaDu tumor-bearing NOD/SCID gamma mice

Based on the above results regarding the favorable cell killing ability of anti-HLA-G CAR-T cells in EGFR variant-expressing FaDu cells, we performed a therapeutic study to further validate its effects. To demonstrate the antitumor activity of anti-HLA-G CAR-T cells in mock, $EGFR^{WT}$, and $EGFR^{L858R}$ FaDu tumor-bearing NOD/SCID gamma mice (NSG) mice, anti-HLA-G CAR-T cells were infused into a xenograft orthotopic OSCC mouse model. For different purposes, the mice were divided into two groups. The survival rate during CAR-T therapy was calculated in group 1. The tumor size in this group was continuously observed using IVIS until the largest diameter of the tumor reached 0.5 cm or when the mice experienced severe aphasia; the other group (group 2) was designed for pathological analysis. The mice in this group were sacrificed on day 21, and the residual tumors from each group were then harvested for IHC staining. The treatment protocol and the images acquired from IVIS were shown in Figure S4. Mock, $EGFR^{WT}$, or $EGFR^{L858R}$-overexpressing FaDu cells were injected into the tongue of the NSG mice, and anti-HLA-G CAR-T cells were then intravenously injected once a week with three doses of rhIL-2. Quantitative results from *in vivo* imaging have shown that the infusion of anti-HLA-G CAR-T cells significantly decreased tumor growth (Figure 6A), and electronic calipers were used to measure tumor volume on day 21 (Figure 6B). Notably, there was no obvious body weight loss during the anti-HLA-G CAR-T therapy (Figure 6C). In addition, gross tumor size (Figure 6D) was also decreased in the anti-HLA-G CAR-T cell-treated mice compared with that in the mock T-treated groups. Metastatic lymph nodes (LN) were also evaluated and were not visible in the anti-HLA-G CAR-T cell-treated $EGFR^{WT}$ and $EGFR^{L858R}$ FaDu tumor-bearing mice on day 21. Furthermore, the survival day of $EGFR^{WT}$ and $EGFR^{L858R}$-overexpressing FaDu tumor-bearing NSG mice administrated with anti-HLA-G CAR-T cells was increased compared with control group, which were observed more than 56 days (Figure 6E). To evaluate the safety of anti-HLA-G CAR-T cells *in vivo*, H&E staining was performed. The results revealed that there was no obvious injury to the vital organs during anti-HLA-G CAR-T cell treatment (Figures 6F and 6G).

To further address the safety using anti-HLA-G CAR-T therapy, we have not only used human normal tissue array chips to confirm the expression levels of HLA-G in vital organs but also examined the cell killing ability within anti-HLA-G CAR-T cell therapy in primary cell cultures. As shown in Figure S5, HLA-G is not detected in vital organs, such as cerebral cortex, cerebellum, skeletal muscle, skin, pancreas, heart, liver, lung, kidney, bladder, and colon. It was only slightly expressed on the cell surface of some macrophages and megakaryocytes in bone marrow, spleen, and thymus. Placenta is a well-characterized positive control for HLA-G IHC staining. In parallel, the protein levels of HLA-G on the surface of normal primary cell cultures were detected, and the cell killing ability of mock T or CAR-T cells on these cells was validated. Human pulmonary fibroblast (HPF; ScienCell, Carlsbad, CA, USA), human renal cortical epithelial cells (HRCE; ATCC), human hepatocytes (HH; ScienCell), human bronchial epithelial cells (HBEpC; Cell Applications, San Diego, CA, USA), human pulmonary microvascular endothelial cells (HPMEC; ScienCell), human corneal epithelial cells (HCEpC; Cell Applications), human umbilical vein endothelial cell (HUVEC; ATCC), and human thymic epithelial cells (HTyEpiC; ScienCell) had slight detectable levels of HLA-G on their cell surface, and there was no significant difference in cell killing between mock T and CAR-T cells

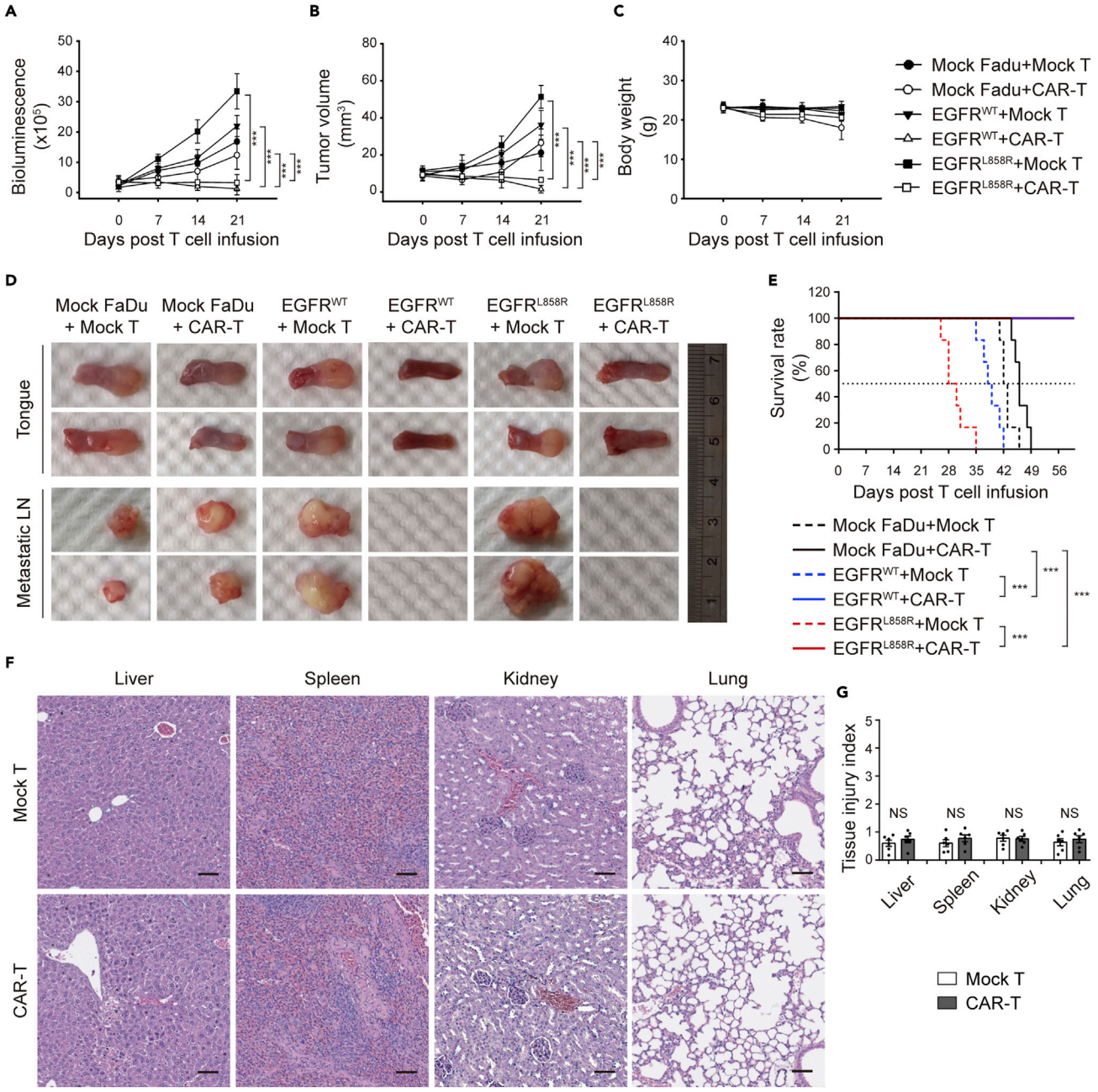

Figure 6. Anti-HLA-G CAR-T cell therapy effectively decreased tumor growth and metastasis in EGFR variants overexpressing FaDu tumor-bearing NSG mice

(A) Tumor progression measured by bioluminescence photometry. The luminoscore was determined as the sum of flux values from the front and back views.

(B) Tumor volume was measured using an electronic manual caliper.

(C) Body weight was measured weekly.

(D) Gross tumor examination for primary tumors and metastatic lymph nodes on day 21.

(E) Mouse survival rate was plotted using the Kaplan-Meier method. Mice were considered dead when the greatest dimension >0.5 cm in any direction, as measured using an electronic manual caliper.

(F) Representative H&E staining for liver, spleen, kidney, and lung was shown in mock T or anti-HLA-G CAR-T cell-treated mice sections.

(G) Quantitative analysis for pathological changes which based on H&E staining was shown as tissue injury index. The data were expressed as the mean ± SEM for six separate experiments. In F, the original magnification was x200. Scale bars, 50 μm ***$p < 0.001$. NS, not significant.

treatment in the primary cell cultures. These results suggest that anti-HLA-G CAR-T cell therapy is safe and effective for the treatment of OSCC cells overexpressing EGFR variants.

Constitutive EGFR activation but not EGFR mutation was the crucial factor for HLA-G expression in FaDu tumor-bearing NSG mice

Although the size of tumors was extremely small or exhibited cancer-free phenotype in anti-HLA-G CAT-T cell-treated groups using IVIS, the residual tumors from the sacrificed mice were collected for further pathological analysis on day 21. As shown in Figure 7A, the expression levels of total EGFR, NLRP3, and HLA-G were highly increased in residual tumors of $EGFR^{WT}$ and $EGFR^{L858R}$ FaDu tumor-bearing NSG mice and the protein levels of $EGFR^{L858R}$ were significantly higher in the $EGFR^{L858R}$ group than in the mock and $EGFR^{WT}$ FaDu groups, consistent with the inoculated cell type. The quantitative results are shown in Figure 7B. The total grading score of total EGFR in OSCC tissues was significantly positively correlated with HLA-G expression ($R = 0.7996$). In parallel, the expression of NLRP3 in OSCC tissues was also significantly positively correlated with HLA-G expression ($R = 0.8152$). However, the total grading score of $EGFR^{L858R}$ in OSCC tissues did not correlate with HLA-G expression ($R = 0.1692$). To provide further evidence, the protein levels of total EGFR, $EGFR^{L858R}$, NLRP3, and HLA-G were determined in tissue samples using Western blot analysis. As shown in Figure 7C, the protein levels of total EGFR, NLRP3, and HLA-G were significantly higher in the $EGFR^{WT}$ and $EGFR^{L858R}$ groups than in the mock FaDu group. Protein levels of $EGFR^{L858R}$ were significantly higher in the $EGFR^{L858R}$ group than in the mock and $EGFR^{WT}$ FaDu groups. All the data presented above suggest that the expression of NLRP3 and HLA-G was highly correlated with over-activated EGFR, while EGFR mutations such as $EGFR^{L858R}$ were not essential for NLRP3 or HLA-G expression in OSCC.

We conducted a series of experiments to address this issue. As shown in Figure S6, the role of $EGFR^{L858R}$ was investigated to clarify the signal transduction of EGFR-HLA-G axis. While $EGFR^{L858R}$ FaDu cells were incubated with or without rhEGF, the protein levels of $EGFR^{L858R}$ and pEGFR did not change in shHLA-G FaDu cells. Simultaneously, to delineate the role of $EGFR^{L858R}$ on HLA-G expression, $EGFR^{L858R}$ in $EGFR^{L858R}$ FaDu cells was knocked down using $EGFR^{L858R}$-specific siRNA. The protein levels of pEGFR and HLA-G markedly increased in rhEGF-treated cells compared to that in untreated cells when $EGFR^{L858R}$ was knocked down in $EGFR^{L858R}$-expressing FaDu cells. These results suggest that constitutive EGFR activation but not EGFR mutation was the crucial factor for HLA-G expression.

DISCUSSION

In this study, we found that anti-HLA-G CAR-T cell therapy could be a potent strategy for EGFR mutated and overexpressed oral cancer. We have verified that EGFR expression was highly correlated with different stages of oral cancer. In addition, either overexpression or mutation of EGFR could increase the expression of MAPK, NLRP3, and HLA-G. This study is the first to demonstrate that HLA-G expression could be induced by EGFR via NLRP3 inflammasome-mediated IL-1β secretion in oral cancer and is a potential target for CAR-T therapy.

Recently, anti-EGFR CAR-T cell therapy has been utilized for treating variant solid tumors, such as triple-negative breast cancer and glioblastoma using mouse model.[50,51] In addition, anti-EGFR and anti-$EGFR^{vIII}$ CAR-T cells have been applied for clinical trial in patients with metastatic pancreatic carcinoma (NCT01869166) and glioblastoma (NCT02209376), respectively.[52,53] However, use of engineered anti-EGFR CAR-T cells against OSCC and their safety assessment is quite limited. The side effects of using anti-EGFR monoclonal antibody in cancer therapies have also been fully investigated.[54,55] For safety concern, although EGFR is constitutively expressed by normal epithelial cells and fibroblast cells, HLA-G is restricted to immune privileged tissues and is barely detected in most adult normal cells except in solid tumors. Therefore, we developed anti-HLA-G CAR-T cells targeting most isoforms of HLA-G. In practice, however, in addition to wild-type EGFR or mutated EGFR targets, our anti-HLA-G CAR-T cells provide an alternative strategy for treating OSCC.

It is worth mentioning that off-target effect is an important safety concern for CAR-T therapy. In normal cells, HLA-G is silenced by epigenetic mechanisms as DNA methylation and histone modification.[56,57] In contrast, tumor cells are shown to express large quantities of HLA-G, which is far greater than normal cells. Although HLA-G has been shown to be inducible by IL-10 and IFN-gamma, it is lightly expressed in normal cells relative to that in tumor cells.[58,59] Previous studies demonstrate that CAR functionality is regulated by the density of target antigen, and low antigen expression contributes to the limitation of

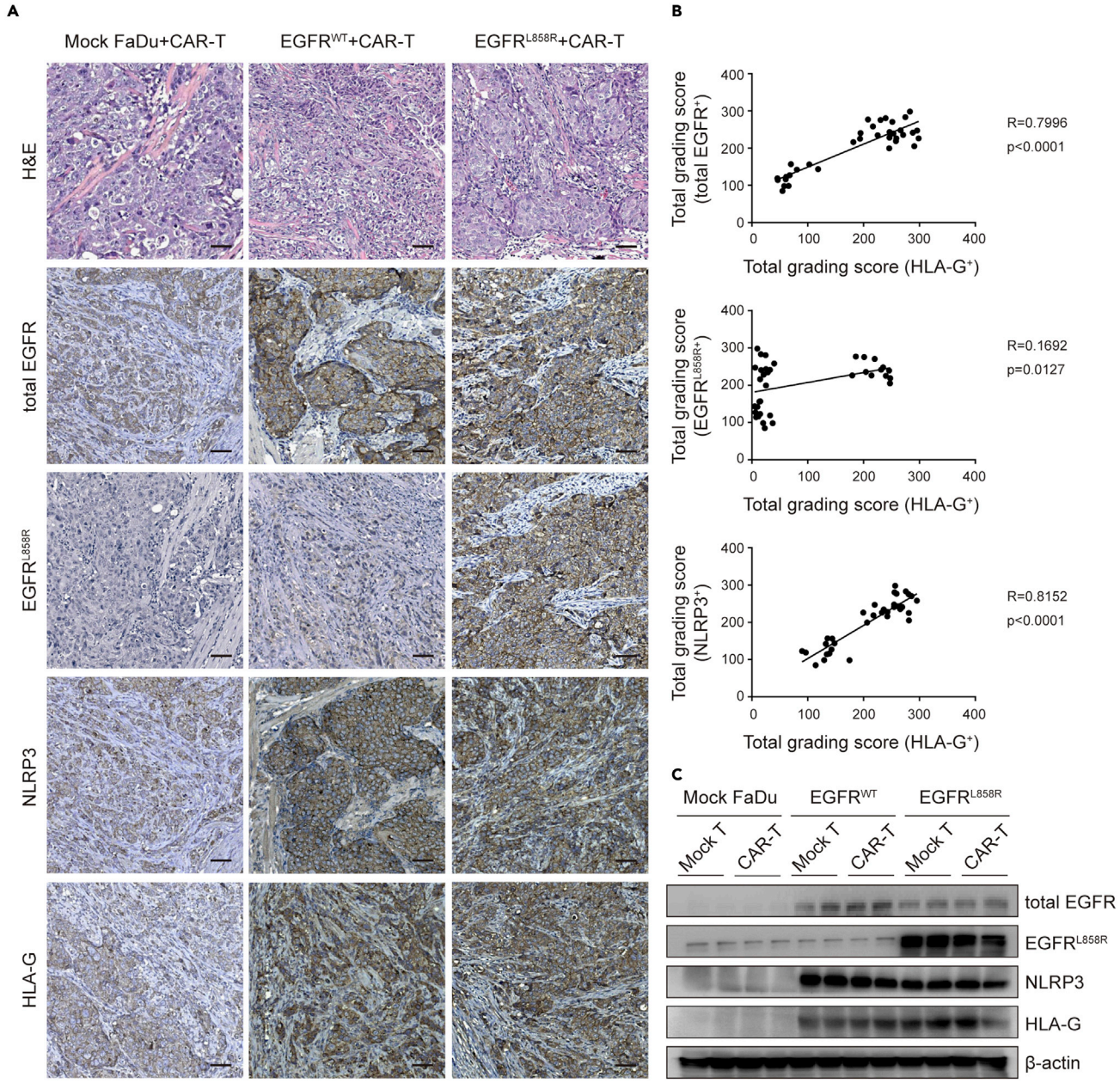

Figure 7. Constitutive EGFR activation but not EGFR mutation was the crucial factor for HLA-G expression in FaDu tumor-bearing NSG mice

Anti-HLA-G CAR-T-treated mice were sacrificed on day 21.

(A) Morphological evaluation by H&E staining. IHC analysis of total EGFR, EGFR^{L858R}, NLRP3, and HLA-G in OSCC tumor lesions.

(B) R values between HLA-G and total EGFR, EGFR^{L858R}, or NLRP3.

(C) Representative Western blot analysis of the levels of total EGFR, EGFR^{L858R}, NLRP3, and HLA-G expression in FaDu tumor-bearing oral tissues. β-actin was used as an internal control. In A, the original magnification was x200. Scale bars, 50 μm.

antitumor efficacy of CAR-T cells.[60,61] Our *in vitro* studies addressed the safety issue in using human normal tissue array chips and examined the cell killing ability within anti-HLA-G CAR-T cell therapy in primary cell cultures. Our animal study has also demonstrated that there was no adverse reaction during anti-HLA-G CAR-T cell treatment. However, it is still difficult to predict off-target effects of CAR-T cells when they are applied to clinical trials. Recently, it is considered that adverse effect through CAR-T therapy can be avoided by adding suicide genes in CAR construct, such as inducible Cas-9 or herpes simplex virus thymidine kinase.[62,63]

In conclusion, our findings showed that EGFR mutants are involved in OSCC tumorigenesis in an NLRP3 inflammasome and HLA-G-dependent manner, which could serve as a specific target for CAR-T therapy. Our *in vitro* and *in vivo* analyses revealed that HLA-G serves as an ideal target for the treatment of OSCC with EGFR variants. We found that over-activated EGFR and specific EGFR mutations induced HLA-G through a MAPK-mediated priming signal of the NLRP3 inflammasome activation pathway in OSCC. Targeting of HLA-G may be a novel therapeutic strategy for deteriorated OSCC. Additional studies are required to determine how the TME is involved in HLA-G CAR-T cell-targeting OSCC using immune complement animals. Combinational therapies may also be considered to promote the antitumor potency of anti-HLA-G cell therapy by overcoming the immunosuppressive TME and enhancing the CAR-T cell response to maximize the cell killing ability against OSCC.

Limitations of the study

There are some limitations in our study, such as relatively small sample size in patient specimens. In addition, it would be better to verify our findings if we can delineate the EGFR-NLRP3-HLA-G axis in transgenic mice or knockout mice.

STAR★METHODS

Detailed methods are provided in the online version of this paper and include the following:

- KEY RESOURCES TABLE
- RESOURCE AVAILABILITY
  - Lead contact
  - Materials availability
  - Data and code availability
- EXPERIMENTAL MODEL AND SUBJECT DETAILS
  - Orthotopic xenotransplantation of FaDu cells in NSG mice for CAR-T cell therapy
- METHOD DETAILS
  - Ethical statement
  - Reagents
  - Patient specimens
  - Safety assessment for anti-HLA-G CAR-T treatment in primary normal cell cultures
  - The production of recombinant HLA-G isoforms in Chinese hamster ovary (CHO) cells
  - Immunohistochemistry
  - Stable overexpression of EGFR variants in FaDu-Luc2 cells
  - Cell viability assay
  - Transwell migration and scratch wound healing assay
  - Cell invasion assay
  - ICC
  - Expansion of primary T cells
  - Transduction of T cells with anti-HLA-G CAR lentiviral practices
  - Flow cytometric analysis
  - Cytotoxic killing assay
  - Short hairpin RNA and small interfering RNA delivery
  - Western blotting
  - ELISA
  - Study approval
- QUANTIFICATION AND STATISTICAL ANALYSIS

SUPPLEMENTAL INFORMATION

Supplemental information can be found online at https://doi.org/10.1016/j.isci.2023.106089.

ACKNOWLEDGMENTS

This study was reviewed and financially supported by previously Ministry of Science and Technology (MOST), now National Science and Technology Council (NSTC) in Taiwan (MOST 110-2314-B-039-052 , NSTC 111-2314-B-039-047, and NSTC 111-2314-B-075B-020-). This work was also supported by the

"Drug Development Center, CMU," from the Featured Areas Research Center Program within the framework of the Higher Education Sprout Project by the Ministry of Education in Taiwan.

AUTHOR CONTRIBUTIONS

Y.-C.L. conceptualized the study. Y.-C.L., S.-W.H., Y.C., C.-H.H., and C.-I.J. designed the methodology. Y.-C.L., C.-C. H., H.-M. L., S.-W.H., Y.C., and F.-Y.L. performed experiments. Y.-C.L., S.-W.H., Y.C., M.-H.T., C.-H.H., F.-Y.L., and P.C. acquired and analyzed the data. Y.-C.L., S.-C.C., W.-H. H., and D.-Y.C. wrote the original draft of the manuscript. All authors reviewed and edited the manuscript. S.-W.H., C.-I.J., S.-C.C., and D.-Y.C. acquired funding for the study. Y.-C.L., C.-H.H., and H.-M.L. contributed equally to this work.

DECLARATION OF INTERESTS

The authors declare no competing interests.

INCLUSION AND DIVERSITY

We support inclusive, diverse, and equitable conduct of research.

Received: June 26, 2022
Revised: November 11, 2022
Accepted: January 25, 2023
Published: January 31, 2023

REFERENCES

1. Jou, A., and Hess, J. (2017). Epidemiology and molecular biology of head and neck cancer. Oncol. Res. Treat. *40*, 328–332.

2. Siegel, R.L., Miller, K.D., Fuchs, H.E., and Jemal, A. (2021). Cancer statistics, 2021. CA. Cancer J. Clin. *71*, 7–33.

3. Singh, P., Barpande, S.R., Bhavthankar, J.D., Mandale, M.S., and Bhagwat, A.U. (2017). Serum Cyfra 21-1 levels in oral squamous cell carcinoma patients and its clinicopathologic correlation. Indian J. Dent. Res. *28*, 162–168.

4. Jung, E.K., Kim, S.-A., Yoon, T.M., Lee, K.-H., Kim, H.K., Lee, D.H., Lee, J.K., Chung, I.-J., Joo, Y.-E., Lim, S.C., et al. (2017). WNT1-inducible signaling pathway protein-1 contributes to tumor progression and treatment failure in oral squamous cell carcinoma. Oncol. Lett. *14*, 1719–1724.

5. Mizrachi, A., Migliacci, J.C., Montero, P.H., McBride, S., Shah, J.P., Patel, S.G., and Ganly, I. (2018). Neck recurrence in clinically node-negative oral cancer: 27-year experience at a single institution. Oral Oncol. *78*, 94–101.

6. Goertzen, C., Mahdi, H., Laliberte, C., Meirson, T., Eymael, D., Gil-Henn, H., and Magalhaes, M. (2018). Oral inflammation promotes oral squamous cell carcinoma invasion. Oncotarget *9*, 29047–29063.

7. Jerjes, W., Upile, T., Petrie, A., Riskalla, A., Hamdoon, Z., Vourvachis, M., Karavidas, K., Jay, A., Sandison, A., Thomas, G.J., et al. (2010). Clinicopathological parameters, recurrence, locoregional and distant metastasis in 115 T1-T2 oral squamous cell carcinoma patients. Head Neck Oncol. *2*, 9.

8. Chinn, S.B., and Myers, J.N. (2015). Oral cavity carcinoma: current management, controversies, and future directions. J. Clin. Oncol. *33*, 3269–3276.

9. Ion, C.M.F., Marasescu, P.C., Matei, M., Florescu, A.M., Margaritescu, C., Petrescu, S.M.S., and Dumitrescu, C.I. (2018). Ion CMF, Marasescu PC, Matei M, et al. Epidemiological and histopathological aspects of tongue squamous cell carcinomas-retrospective study. Curr. Health Sci. J. *44*, 211–224.

10. Zhang, Y., Jin, X., and Wang, J. (2019). miR-148a modulates the viability, migration and invasion of oral squamous cell carcinoma cells by regulating HLA-G expression. Mol. Med. Rep. *20*, 795–801.

11. Biteghe, F.A.N., Mungra, N., Chalomie, N.E.T., Ndong, J.D.L.C., Engohang-Ndong, J., Vignaux, G., Padayachee, E., Naran, K., and Barth, S. (2020). Advances in epidermal growth factor receptor specific immunotherapy: lessons to be learned from armed antibodies. Oncotarget *11*, 3531–3557.

12. Jureczek, J., Feldmann, A., Bergmann, R., Arndt, C., Berndt, N., Koristka, S., Loureiro, L.R., Mitwasi, N., Hoffmann, A., Kegler, A., et al. (2020). Highly efficient targeting of EGFR-expressing tumor cells with uniCAR T cells via target modules based on Cetuximab. Onco Targets Ther. *13*, 5515–5527.

13. Takahashi, K., Ishibashi, E., Kubo, T., Harada, Y., Hayashi, H., Kano, M., Shimizu, Y., Shirota, H., Mori, Y., Muto, M., et al. (2020). A phase 2 basket trial of combination therapy with trastuzumab and pertuzumab in patients with solid cancers harboring human epidermal growth factor receptor 2 amplification (JUPITER trial). Medicine (Baltim.) *99*, e21457.

14. Alorabi, M., Shonka, N.A., and Ganti, A.K. (2016). EGFR monoclonal antibodies in locally advanced head and neck squamous cell carcinoma: what is their current role? Crit. Rev. Oncol. Hematol. *99*, 170–179.

15. Costa, V., Kowalski, L.P., Coutinho-Camillo, C.M., Begnami, M.D., Calsavara, V.F., Neves, J.I., and Kaminagakura, E. (2018). EGFR amplification and expression in oral squamous cell carcinoma in young adults. Int. J. Oral Maxillofac. Surg. *47*, 817–823.

16. Leong, H.S., Chong, F.T., Sew, P.H., Lau, D.P., Wong, B.H., Teh, B.-T., Tan, D.S.W., and Iyer, N.G. (2014). Targeting cancer stem cell plasticity through modulation of epidermal growth factor and insulin-like growth factor receptor signaling in head and neck squamous cell cancer. Stem Cells Transl. Med. *3*, 1055–1065.

17. Gupta, S., Khan, H., Kushwaha, V.S., Husain, N., Negi, M., Ghatak, A., and Bhatt, M. (2015). Impact of EGFR and p53 expressions on survival and quality of life in locally advanced oral squamous cell carcinoma patients treated with chemoradiation. Cancer Biol. Ther. *16*, 1269–1280.

18. Gupta, S., Kushwaha, V.S., Verma, S., Khan, H., Bhatt, M.L.B., Husain, N., Negi, M.P.S., Bhosale, V.V., and Ghatak, A. (2016). Understanding molecular markers in recurrent oral squamous cell carcinoma treated with chemoradiation. Heliyon *2*, e00206.

19. Sarkis, S.A., Abdullah, B.H., Abdul Majeed, B.A., and Talabani, N.G. (2010). Immunohistochemical expression of epidermal growth factor receptor (EGFR) in oral squamous cell carcinoma in relation to

proliferation, apoptosis, angiogenesis and lymphangiogenesis. Head Neck Oncol. *2*, 13.

20. Goel, B., Tiwari, A.K., Pandey, R.K., Singh, A.P., Kumar, S., Sinha, A., Jain, S.K., and Khattri, A. (2022). Therapeutic approaches for the treatment of head and neck squamous cell carcinoma-An update on clinical trials. Transl. Oncol. *21*, 101426. https://doi.org/10.1016/j.tranon.2022.101426.

21. Zibelman, M., and Mehra, R. (2016). Overview of current treatment options and investigational targeted therapies for locally advanced squamous cell carcinoma of the head and neck. Am. J. Clin. Oncol. *39*, 396–406. https://doi.org/10.1097/COC.0000000000000283.

22. Huang, S.-F., Chuang, W.-Y., Chen, I.-H., Liao, C.-T., Wang, H.-M., and Hsieh, L.-L. (2009). EGFR protein overexpression and mutation in areca quid-associated oral cavity squamous cell carcinoma in Taiwan. Head Neck *31*, 1068–1077.

23. Lee, J.W., Soung, Y.H., Kim, S.Y., Nam, H.K., Park, W.S., Nam, S.W., Kim, M.S., Sun, D.I., Lee, Y.S., Jang, J.J., et al. (2005). Somatic mutations of EGFR gene in squamous cell carcinoma of the head and neck. Clin. Cancer Res. *11*, 2879–2882.

24. Peng, W., Pu, X., Jiang, M., Wang, J., Li, J., Li, K., Xu, Y., Xu, F., Chen, B., Wang, Q., et al. (2021). Dacomitinib induces objective responses in metastatic brain lesions of patients with EGFR-mutant non-small-cell lung cancer: a brief report. Lung Cancer *152*, 66–70.

25. Troiano, G., Rubini, C., Togni, L., Caponio, V.C.A., Zhurakivska, K., Santarelli, A., Cirillo, N., Lo Muzio, L., and Mascitti, M. (2020). The immune phenotype of tongue squamous cell carcinoma predicts early relapse and poor prognosis. Cancer Med. *9*, 8333–8344.

26. Wolf, G.T., Liu, S., Bellile, E., Sartor, M., Rozek, L., Thomas, D., Nguyen, A., Zarins, K., and McHugh, J.B.; INSPIRE Trial Clinical Investigators (2020). Tumor infiltrating lymphocytes after neoadjuvant IRX-2 immunotherapy in oral squamous cell carcinoma: interim findings from the INSPIRE trial. Oral Oncol. *111*, 104928.

27. Wu, W., Wages, P.A., Devlin, R.B., Diaz-Sanchez, D., Peden, D.B., and Samet, J.M. (2015). SRC-mediated EGF receptor activation regulates ozone-induced interleukin 8 expression in human bronchial epithelial cells. Environ. Health Perspect. *123*, 231–236.

28. Allen, I.C., Lich, J.D., Arthur, J.C., Jania, C.M., Roberts, R.A., Callaway, J.B., Tilley, S.L., and Ting, J.P.-Y. (2012). Characterization of NLRP12 during the development of allergic airway disease in mice. PLoS One *7*, e30612.

29. Lu, B., Nakamura, T., Inouye, K., Li, J., Tang, Y., Lundbäck, P., Valdes-Ferrer, S.I., Olofsson, P.S., Kalb, T., Roth, J., et al. (2012). Novel role of PKR in inflammasome activation and HMGB1 release. Nature *488*, 670–674.

30. Ogino, K., Zhang, R., Takahashi, H., Takemoto, K., Kubo, M., Murakami, I., Wang, D.H., and Fujikura, Y. (2014). Allergic airway inflammation by nasal inoculation of particulate matter (PM2.5) in NC/Nga mice. PLoS One *9*, e92710.

31. Latz, E., Xiao, T.S., and Stutz, A. (2013). Activation and regulation of the inflammasomes. Nat. Rev. Immunol. *13*, 397–411.

32. Ma, Z.-Z., Sun, H.-S., Lv, J.-C., Guo, L., and Yang, Q.-R. (2018). Expression and clinical significance of the NEK7-NLRP3 inflammasome signaling pathway in patients with systemic lupus erythematosus. J. Inflamm. *15*, 16.

33. Vanaja, S.K., Rathinam, V.A.K., and Fitzgerald, K.A. (2015). Mechanisms of inflammasome activation: recent advances and novel insights. Trends Cell Biol. *25*, 308–315.

34. Feng, X., Luo, Q., Zhang, H., Wang, H., Chen, W., Meng, G., and Chen, F. (2017). The role of NLRP3 inflammasome in 5-fluorouracil resistance of oral squamous cell carcinoma. J. Exp. Clin. Cancer Res. *36*, 81.

35. Li, Z., Liu, F.-Y., and Kirkwood, K.L. (2020). The p38/MKP-1 signaling axis in oral cancer: impact of tumor-associated macrophages. Oral Oncol. *103*, 104591.

36. Mortezaee, K. (2020). Immune escape: a critical hallmark in solid tumors. Life Sci. *258*, 118110.

37. Shi, G.-M., Wang, J., Huang, X.-W., Huang, X.-Y., He, Y.-F., Ji, Y., Chen, Y., Wu, D., Lu, J.-C., Sun, Q.-M., et al. (2021). Graft PD-L1 expression as a marker for transplant rejection following anti-PD1 immunotherapy for recurrent liver tumors. Liver Transpl. *27*, 444–449.

38. Simatou, A., Sarantis, P., Koustas, E., Papavassiliou, A.G., and Karamouzis, M.V. (2020). The role of the RANKL/RANK axis in the prevention and treatment of breast cancer with immune checkpoint inhibitors and anti-RANKL. Int. J. Mol. Sci. *21*, E7570.

39. Bian, X., Si, Y., Zhang, M., Wei, R., Yang, X., Ren, H., Zheng, G., Wang, C., and Zhang, Y. (2016). Down-expression of miR-152 lead to impaired anti-tumor effect of NK via upregulation of HLA-G. Tumour Biol. *37*, 3749–3756.

40. Lin, A., and Yan, W.H. (2018). Heterogeneity of HLA-G expression in cancers: facing the challenges. Front. Immunol. *9*, 2164.

41. Shahrabi, S., Hadad, E.H., Asnafi, A.A., Behzad, M.M., Ehsanpour, A., and Saki, N. (2019). Human leukocyte antigens in cancer metastasis: prognostic approach and therapeutic susceptibility. Histol. Histopathol. *34*, 111–124.

42. Siu, D. (2009). Cancer therapy using tumor-associated antigens to reduce side effects. Clin. Exp. Med. *9*, 181–198.

43. Bell, R.B. (2016). The fourth modality: immunotherapy for head and neck cancer hits pay dirt. Oral Surg. Oral Med. Oral Pathol. Oral Radiol. *121*, 575–577.

44. Carosella, E.D., Ploussard, G., LeMaoult, J., and Desgrandchamps, F. (2015). A systematic review of immunotherapy in urologic cancer: evolving roles for targeting of CTLA-4, PD-1/PD-L1, and HLA-G. Eur. Urol. *68*, 267–279.

45. Homet Moreno, B., and Ribas, A. (2015). Anti-programmed cell death protein-1/ligand-1 therapy in different cancers. Br. J. Cancer *112*, 1421–1427.

46. Wang, H., Luo, Q., Feng, X., Zhang, R., Li, J., and Chen, F. (2018). NLRP3 promotes tumor growth and metastasis in human oral squamous cell carcinoma. BMC Cancer *18*, 500.

47. Dou, Z., Gao, L., Ren, W., Zhang, H., Wang, X., Li, S., Zheng, J., Kong, X., Chi, P., and Zhi, K. (2020). CiRS-7 functions as a ceRNA of RAF-1/PIK3CD to promote metastatic progression of oral squamous cell carcinoma via MAPK/AKT signaling pathways. Exp. Cell Res. *396*, 112290.

48. Lin, W.-W., Lu, Y.-C., Huang, B.-C., Chuang, C.-H., Cheng, Y.-A., Chen, I.-J., Liu, H.-J., Ho, K.-W., Liao, T.-Y., Liu, E.-S., et al. (2021). Selective activation of pro-anti-IL-1β antibody enhances specificity for autoinflammatory disorder therapy. Sci. Rep. *11*, 14846.

49. Marchetti, C., Swartzwelter, B., Gamboni, F., Neff, C.P., Richter, K., Azam, T., Carta, S., Tengesdal, I., Nemkov, T., D'Alessandro, A., et al. (2018). OLT1177, a β-sulfonyl nitrile compound, safe in humans, inhibits the NLRP3 inflammasome and reverses the metabolic cost of inflammation. Proc. Natl. Acad. Sci. USA *115*, E1530–E1539.

50. Jiang, H., Gao, H., Kong, J., Song, B., Wang, P., Shi, B., Wang, H., and Li, Z. (2018). Selective targeting of glioblastoma with EGFRvIII/EGFR bitargeted chimeric antigen receptor T cell. Cancer Immunol. Res. *6*, 1314–1326.

51. Liu, Y., Zhou, Y., Huang, K.H., Li, Y., Fang, X., An, L., Wang, F., Chen, Q., Zhang, Y., Shi, A., et al. (2019). EGFR-specific CAR-T cells trigger cell lysis in EGFR-positive TNBC. Aging (Albany NY) *11*, 11054–11072.

52. Johnson, L.A., Scholler, J., Ohkuri, T., Kosaka, A., Patel, P.R., McGettigan, S.E., Nace, A.K., Dentchev, T., Thekkat, P., Loew, A., et al. (2015). Rational development and characterization of humanized anti-EGFR variant III chimeric antigen receptor T cells for glioblastoma. Sci. Transl. Med. *7*, 275ra22.

53. Liu, Y., Guo, Y., Wu, Z., Feng, K., Tong, C., Wang, Y., Dai, H., Shi, F., Yang, Q., and Han, W. (2020). Anti-EGFR chimeric antigen receptor-modified T cells in metastatic pancreatic carcinoma: A phase I clinical trial. Cytotherapy *22*, 573–580.

54. Li, J., and Yan, H. (2018). Skin toxicity with anti-EGFR monoclonal antibody in cancer patients: a meta-analysis of 65 randomized controlled trials. Cancer Chemother. Pharmacol. *82*, 571–583.

55. Su, X., Lacouture, M.E., Jia, Y., and Wu, S. (2009). Risk of high-grade skin rash in cancer patients treated with cetuximab-an antibody against epidermal growth factor

receptor: systemic review and meta-analysis. Oncology *77*, 124–133.

56. Onno, M., Guillaudeux, T., Amiot, L., Renard, I., Drenou, B., Hirel, B., Girr, M., Semana, G., Le Bouteiller, P., and Fauchet, R. (1994). The HLA-G gene is expressed at a low mRNA level in different human cells and tissues. Hum. Immunol. *41*, 79–86.

57. Polakova, K., Bandzuchova, E., Tirpakova, J., Kuba, D., and Russ, G. (2007). Modulation of HLA-G expression. Neoplasma *54*, 455–462.

58. Moreau, P., Adrian-Cabestre, F., Menier, C., Guiard, V., Gourand, L., Dausset, J., Carosella, E.D., and Paul, P. (1999). IL-10 selectively induces HLA-G expression in human trophoblasts and monocytes. Int. Immunol. *11*, 803–811.

59. Yang, Y., Chu, W., Geraghty, D.E., and Hunt, J.S. (1996). Expression of HLA-G in human mononuclear phagocytes and selective induction by IFN-gamma. J. Immunol. *156*, 4224–4231.

60. Majzner, R.G., Rietberg, S.P., Sotillo, E., Dong, R., Vachharajani, V.T., Labanieh, L., Myklebust, J.H., Kadapakkam, M., Weber, E.W., Tousley, A.M., et al. (2020). Tuning the antigen density requirement for CAR T-cell activity. Cancer Discov. *10*, 702–723.

61. Rodriguez-Marquez, P., Calleja-Cervantes, M.E., Serrano, G., Oliver-Caldes, A., Palacios-Berraquero, M.L., Martin-Mallo, A., Calviño, C., Español-Rego, M., Ceballos, C., Lozano, T., et al. (2022). CAR density influences antitumoral efficacy of BCMA CAR T cells and correlates with clinical outcome. Sci. Adv. *8*, eabo0514.

62. Ghaffari, S., Khalili, N., and Rezaei, N. (2021). CRISPR/Cas9 revitalizes adoptive T-cell therapy for cancer immunotherapy. J. Exp. Clin. Cancer Res. *40*, 269.

63. Jones, B.S., Lamb, L.S., Goldman, F., and Di Stasi, A. (2014). Improving the safety of cell therapy products by suicide gene transfer. Front. Pharmacol. *5*, 254.

64. Almangush, A., Mäkitie, A.A., Triantafyllou, A., de Bree, R., Strojan, P., Rinaldo, A., Hernandez-Prera, J.C., Suárez, C., Kowalski, L.P., Ferlito, A., et al. (2020). Staging and grading of oral squamous cell carcinoma: an update. Oral Oncol. *107*, 104799.

65. Seoane-Romero, J.-M., Vázquez-Mahía, I., Seoane, J., Varela-Centelles, P., Tomás, I., and López-Cedrún, J.L. (2012). Factors related to late stage diagnosis of oral squamous cell carcinoma. Med. Oral Patol. Oral Cir. Bucal *17*, e35–e40.

66. Lin, Y.-C., Hwu, Y., Huang, G.-S., Hsiao, M., Lee, T.-T., Yang, S.-M., Lee, T.-K., Chen, N.-Y., Yang, S.-S., Chen, A., et al. (2017). Differential synchrotron X-ray imaging markers based on the renal microvasculature for tubulointerstitial lesions and glomerulopathy. Sci. Rep. *7*, 3488.

67. Sordella, R., Bell, D.W., Haber, D.A., and Settleman, J. (2004). Gefitinib-sensitizing EGFR mutations in lung cancer activate anti-apoptotic pathways. Science *305*, 1163–1167.

68. El-Mezzein, R.E., Matsumoto, T., Nomiyama, H., and Miike, T. (2001). Increased secretion of IL-18 in vitro by peripheral blood mononuclear cells of patients with bronchial asthma and atopic dermatitis. Clin. Exp. Immunol. *126*, 193–198.

STAR★METHODS

KEY RESOURCES TABLE

REAGENT or RESOURCE	SOURCE	IDENTIFIER
Antibodies		
Recombinant Anti-EGFR antibody [EP38Y]	Abcam	Cat# ab52894, RRID: AB_869579
EGF Receptor (L858R Mutant Specific) [43B2]	Cell Signaling Technology	Cat# 3197, RRID: AB_1903955
Anti-NLRP3/NALP3, mAb [Cryo-2]	Adipogen Life Sciences	Cat# AG-20B-0014-C100, RRID: AB_2885199
Anti-HLA-G antibody [4H84]	Santa Cruz Biotechnology	Cat# sc-21799, RRID: AB_627938
Anti-pan Cadherin antibody	GeneTex	Cat# GTX132646, RRID: AB_2886698
Goat anti-rabbit IgG H&L, Alexa Fluor 647	Abcam	Cat# ab150079, RRID: AB_2722623
FITC Anti-CD3 epsilon antibody [OKT3]	Abcam	Cat# ab210316, RRID: N/A
Streptavidin, Alexa Fluor™ 647 conjugate	Thermo Fisher Scientific	Cat# S21374, RRID: AB_2336066
HLA-G monoclonal antibody [87G], PE	Thermo Fisher Scientific	Cat# 12-9957-42, RRID: AB_448029
Anti-EGFR (phospho Y1068) antibody	Abcam	Cat# ab5644, RRID: AB_305012
EGF Receptor (E746-A750del Specific) [D6B6]	Cell Signaling Technology	Cat# 2085, RRID: AB_1903953
EGFR Antibody [DH8.3] - EGFRvIII	Novus Biologicals	Cat# NBP2-50599
Phospho-p44/42 MAPK (Erk1/2) (Thr202/Tyr204) [D13.14.4E]	Cell Signaling Technology	Cat# 4370, RRID: AB_2315112
p44/42 MAPK (Erk1/2) [137F5]	Cell Signaling Technology	Cat# 4695, RRID: AB_390779
Phospho-SAPK/JNK (Thr183/Tyr185) Antibody	Cell Signaling Technology	Cat# 9251, RRID: AB_331659
SAPK/JNK Antibody	Cell Signaling Technology	Cat# 9252, RRID: AB_2250373
Phospho-p38 MAPK (Thr180/Tyr182) [D3F9]	Cell Signaling Technology	Cat# 4511, RRID: AB_2139682
p38 MAPK Antibody	Cell Signaling Technology	Cat# 9212, RRID: AB_330713
Human IL-1 beta /IL-1F2 Antibody [Clone 8516]	R&D Systems	Cat# MAB201, RRID: AB_358006
E-Cadherin antibody	GeneTex	Cat# GTX100443, RRID: AB_10729586
Vimentin antibody [GT7812]	GeneTex	Cat# GTX629743, RRID: AB_2888145
β-actin	GeneTex	Cat# GTX109639, RRID: AB_1949572

(*Continued on next page*)

Continued

REAGENT or RESOURCE	SOURCE	IDENTIFIER
HRP-conjugated mouse anti-rabbit IgG antibody	Santa Cruz Biotechnology	Cat# sc-2357, RRID: AB_628497
HRP-conjugated m-IgGκ BP	Santa Cruz Biotechnology	Cat# sc-516102, RRID: AB_2687626
Ultra-LEAF purified anti-human HLA-G Antibody [87G]	BioLegend	Cat# 335924, RRID: AB_2810515
HLA-G antibody [MEM-G/9]	GeneTex	Cat# GTX27758, RRID: AB_371650
Biological samples		
Normal Tissue Array	Pantomics Inc	Cat# MNO1021, RRID: N/A
Chemicals, peptides, and recombinant proteins		
Puromycin solution	InvivoGen	Cat# ant-pr, RRID: N/A
Blasticidin	InvivoGen	Cat# ant-bl, RRID: N/A
Polybrene	Santa Cruz Biotechnology	Cat# sc-134220, RRID: N/A
PD98059 (CAS 167869-21-8)	Santa Cruz Biotechnology	Cat# sc-3532, RRID: N/A
DMSO	Sigma-Aldrich	Cat# D8418, RRID: N/A
Dapansutrile	Selleck Chemicals	Cat# S8907, RRID: N/A
Canakinumab	R&D Systems	Cat# MAB10349, RRID: N/A
Protein L	Sigma-Aldrich	Cat# P3101, RRID: N/A
Citrate sodium buffer	Sigma-Aldrich	Cat# S7899, RRID: N/A
Bovine Serum Albumin	Sigma-Aldrich	Cat# A7030, RRID: N/A
3, 3′-diaminobenzidine	Dako	Cat# K3468, RRID: N/A
Lipofectamine 3000	Invitrogen	Cat# L300015, RRID: N/A
Lipopolysaccharides from *Escherichia coli* O111:B4	Sigma-Aldrich	Cat# L4391, RRID: N/A
MTT Formazan	Sigma-Aldrich	Cat# M2003, RRID: N/A
crystal violet (Sigma-Aldrich).	Sigma-Aldrich	Cat# C0775, RRID: N/A
Mitomycin C	Sigma-Aldrich	Cat# M4287, RRID: N/A
Matrigel	BD Biosciences	Cat# 354234, RRID: N/A
ProLong gold antifade mountant with DAPI	Thermo Fisher Scientific	Cat# P36931, RRID: N/A

(*Continued on next page*)

Continued

REAGENT or RESOURCE	SOURCE	IDENTIFIER
Recombinant human IL-2	PeproTech	Cat# AF-200-02, RRID: N/A
Recombinant Human IL-1 beta/IL-1F2 Protein	R&D Systems	Cat# 201-LB-005/CF, RRID: N/A
CellTracker™ Green CMFDA Dye	Thermo Fisher Scientific	Cat# C2925, RRID: N/A
Propidium iodide solution	Sigma-Aldrich	Cat# P4864, RRID: N/A
PRO-PREP protein extraction buffer	iNtRON Biotechnology	Cat# 17081, RRID: N/A
RPMI 1640 medium	Thermo Fisher Scientific	Cat# 11875085, RRID: N/A
EMEM	Thermo Fisher Scientific	Cat# 11095098, RRIP: N/A
ExpiCHO™ Expression Medium	Thermo Fisher Scientific	Cat# A2910001, RRIP: N/A
Recombinant Human HLA-G Protein, His-Avi-tagged	Creative BioMart	Cat# HLA-G-312H, RRIP: N/A
Coomassie brilliant blue R-250 staining solution	Bio-Rad	Cat# 1610436, RRID: N/A
Critical commercial assays		
EasySep™ Human T Cell Isolation Kit	STEMCELL Technologies	Cat# 17951, RRID: N/A
Human IL-1 beta/IL-1F2 Quantikine ELISA Kit	R&D Systems	Cat# DLB50, RRID: N/A
Human IL-18 ELISA Kit	ABclonal	Cat# RK00176, RRID: N/A
Bradford protein assay	Thermo Fisher Scientific	Cat# 23236, RRID: N/A
Western lightning plus, chemiluminescent substrate	PerkinElmer	Cat# NEL105001EA, RRID: N/A
Experimental models: Cell lines		
FaDu-Luc2	ATCC	Cat# HTB-43-LUC2, RRID: N/A
Human pulmonary fibroblast	ScienCell	Cat# 3300, RRID: N/A
Human renal cortical epithelial cells	ATCC	Cat# PCS-400-011, RRID: N/A
Human hepatocytes	ScienCell	Cat# 5200, RRID: N/A
Human bronchial epithelial cells	Cell Applications	Cat# 502-05a, RRID: N/A
Human pulmonary microvascular endothelial cells	ScienCell	Cat# 3000, RRID: N/A
Human corneal epithelial cells	Cell Applications	Cat# 630-05a, RRID: N/A
Human umbilical vein endothelial cell	ATCC	Cat# PCS-100-010, RRID: N/A

(*Continued on next page*)

Continued

REAGENT or RESOURCE	SOURCE	IDENTIFIER
Human thymic epithelial cells	ScienCell	Cat# 3910, RRID: N/A
ExpiCHO-S™ Cells	Thermo Fisher Scientific	Cat# A29127, RRID: CVCL_4W07
Experimental models: Organisms/strains		
Mouse: NOD.Cg-*Prkdc*^{scid} *Il2rg*^{tm1Wjl}/SzJ	The Jackson Laboratory	Cat# JAX:005557, RRID: IMSR_JAX:005557
Oligonucleotides		
EGFR shRNA Plasmid (h)	Santa Cruz Biotechnology	Cat# sc-29301-SH, RRID: N/A
HLA-G shRNA Plasmid (h)	Santa Cruz Biotechnology	Cat# sc-42920-SH, RRID: N/A
Cryopyrin/NALP3/NLRP3 shRNA Plasmid (h)	Santa Cruz Biotechnology	Cat# sc-45469-SH, RRID: N/A
EGFR^{L858R} siRNA (Customization)	Qiagen	Cat# N/A, RRID: N/A
HLA-G isoforms (Customization)	GenScript	Cat# N/A, RRID: N/A
Recombinant DNA		
EGFR WT plasmids	Addgene	Cat# 11011, RRID: Addgene_11011
pBabe EGFR Del1	Addgene	Cat# 32062, RRID: Addgene_32062
EGFR L858R	Addgene	Cat# 11012, RRID: Addgene_11012
MSCV-XZ066-EGFRvIII plasmids	Addgene	Cat# 20737, RRID: Addgene_20737
Software and algorithms		
Live Image, Version 4.7.1(IVIS imaging)	Perkin Elmer	N/A
PAX-it software, Version 7.4	Midwest Information Systems	N/A
ImageJ software, Version 1.46;	National Institutes of Health	N/A
Other		
Attane (Isoflurane)	Baxter Healthcare	ATC: N01AB06
Zoletil	Virbac	ATC: QN01AX99

RESOURCE AVAILABILITY

Lead contact

Further information and requests for resources and reagents should be directed to and will be fulfilled by the lead contact, Chia-Ing Jan (janc1206@yahoo.com.tw).

Materials availability

EGFR variants overexpressing FaDu cells generated in this study are available from the lead contact upon request with a completed Materials Transfer Agreement.

Data and code availability

All data supporting the findings of this study are available within the main manuscript and the supplementary files. This paper does not report original code. The software used in this study is described in the above

section and the key resources table in details. Any additional information required to reanalyze the data reported in this paper is available from the lead contact upon request.

EXPERIMENTAL MODEL AND SUBJECT DETAILS

Orthotopic xenotransplantation of FaDu cells in NSG mice for CAR-T cell therapy

Mock, $EGFR^{WT}$ and $EGFR^{L858R}$ overexpressed FaDu cells were harvested for the orthotopic xenograft OSCC mouse model. Briefly, the cells were washed and resuspended in PBS mixed with Matrigel (BD Biosciences, 1:1) at a density of 1×10^6 cells/mL. Male NSG mice (6-8 weeks old) were anesthetized by intraperitoneal injection of zoletil (40 mg/kg), and FaDu cells were then inoculated orthotopically near the base of the tongue. Mice were allowed to rest in individual cages for at least 30 min for recovery after delivery. Seven days after cell implantation, the mice were infused intravenously with mock or anti-HLA-G CAR-T cells (5×10^6 cells/mouse). Two additional infusions of mock or anti-HLA-G CAR-T cells (5×10^6 cells/mouse) were started after the first infusion (once a week). Tumor growth and regional lymph node metastasis were monitored weekly using an IVIS spectrum novel patented optical imaging system (PerkinElmer) with a bioluminescence channel. In addition, tumor volume was evaluated using digital calipers and calculated. Tumor volume (TV) was calculated using the following formula: TV (mm^3) = ($Length^2 \times Width$) /2. The mice were sacrificed when the largest diameter of the tumor reached 0.5 cm or when the mice experienced severe aphagosis. Tumors were harvested, their sizes and weights were measured, and gross tumor images were taken. The tissue injury index was used to evaluate the safety of anti-HLA-G CAR-T therapy based on H&E staining. Briefly, the liver, spleen, kidney, and lung tissues were harvested on day 21. The tissue samples were then processed for H&E staining and observed under a light microscope. Injuries were characterized by diffuse reactions in the interstitial areas, including neutrophil infiltration, necrosis, cytoplasmic vacuoles, hemorrhage, atrophy, and abnormal dilatation. Higher scores represent more severe tissue damage in our scoring system: 0, no observed histopathological changes; 1, < 10%; 2, 10–25%; 3, 25–50%; 4, 50–75%, 5, 75–100 %. All slides were reviewed blindly and scored independently by two pathologists using an optical microscope at 200 × magnification.

METHOD DETAILS

Ethical statement

Mice were obtained from the National Laboratory Animal Center and housed at China Medical University (CMU), Taichung, Taiwan. Mice with a mean weight of 20 g were used as the xenograft OSCC tumor model, and the mice were healthy before cell transplantation. The mice were kept in individual ventilated cages and kept at 24 ± 2°C with 40 to 70% humidity on a 12 h light/dark cycle under specific pathogen-free conditions.

Reagents

Reagents, including puromycin and blasticidin, were acquired from InvivoGen (San Diego, CA, USA). Polybrene was obtained from Santa Cruz Biotechnology (Dallas, TX). The inhibitors, PD98059 was obtained from Santa Cruz Biotechnology and dissolved in DMSO (Sigma-Aldrich, St. Louis, MO, USA). Dapansutrile (OLT117) was obtained from Selleck Chemicals (Houston, TX, USA), and canakinumab (Ilaris) was obtained from R&D Systems (Minneapolis, MN, USA). RhEGF was purchased from R&D Systems. Protein L was obtained from Sigma-Aldrich. HLA-G blocking/neutralizing antibody (clone 87G) was obtained from BioLegend (San Diego, CA, USA).

Patient specimens

Information on patients with OSCC, including TNM clinical staging, metastasis, progression-free survival, and OS, was obtained from their medical records. Microscopic characteristics were assessed using tissue sections stained with H&E. OSCC samples were then graded based on the criteria described by the World Health Organization (WHO) classification of tumors and the American Joint Committee on Cancer (AJCC) manual for staging cancer.[64] Two pathologists independently graded epithelial dysplasia and classified each sample. Fifty-six OSCC patients (54 men and 2 women, aged between 44 to 62 years old) underwent operative treatment and their data were collected at China Medical University Hospital (CMUH), Taiwan. At the same time, the adjacent tissues from patients without tumors were used as a matched group. According to the classification of malignant tumors, patients were classified into stages I ($n = 13$), II ($n = 11$), III ($n = 11$), and IV ($n = 21$). All tissue specimens were fixed in formalin and embedded in paraffin for immunostaining. Samples from stages I and II were grouped together and referred to as "early stage," and samples from stages III and IV were

grouped as "late stage".[65] For statistical analysis, Pearson's correlation analysis was used to calculate the R-values for the correlation between staining intensity scores and tumor staging. Statistical significance was considered when the *p*-value was <0.05. Gender does not influence on the results of this study. Normal tissue arrays were purchased to evaluate the expression levels of HLA-G in other tissues (Pantomics, Fairfield, CA, USA).

Safety assessment for anti-HLA-G CAR-T treatment in primary normal cell cultures

Some common non-tumor primary normal cells were purchased to examine the expression levels of HLA-G as well as the cell killing ability within anti-HLA-G CAR-T cell therapy in primary cell cultures. In brief, HPF, HRCE, HH, HBEpC, HPMEC, HCEpC, HUVEC, and HTyEpiC were obtained and cultured in their recommended medium at 37 °C in the presence of 5% CO_2. To further evaluate the cell killing ability of anti-HLA-G CAR-T in these normal cells, cytotoxic killing assay was performed. The mock and anti-HLA-G CAR T cells were co-cultured with CellTracker Green stained normal cells at ratios of 1:1, 3:1, and 6:1 in 1 mL of medium with IL-2 (100 U/mL) for 24, 48, and 72 h at 37 °C. The control groups contained only normal cells. The co-cultured cells were stained with PI. The presence of granules and PI populations were considered as dead cells. Cell killing ability was presented as the percentage of normal cell death in the total cell population.

The production of recombinant HLA-G isoforms in Chinese hamster ovary (CHO) cells

The nucleotide sequence encoding HLA-G isoforms (accession number of full-length HLA-G is NM_001363567.2) were synthesized, amplified, and subcloned into pcDNA3.4 vector (GenScript, Nanjing, Jiangsu, China). To obtain recombinant HLA-G isoforms, the supernatants from transfected ExpiCHO-S cells (Thermo Fisher Scientific) were collected and HLA-G isoforms were then purified in a two-step process using protein A chromatography followed by gel filtration. The molecular weights of HLA-G isoforms were determined using Coomassie blue staining. Besides, the full-length of HLA-G recombinant protein containing β_2-microglobulin (G1 and G5) was purchased from Creative BioMart (Shirley, NY, USA). The binding ability of these isoforms to commercial HLA-G antibodies (clone 87G, 4H84, and MEM-G/9) were further pre-confirmed by ELISA assay.

Immunohistochemistry

IHC analysis was performed on 3 μm thick sections. Briefly, tissue sections were mounted on polylysine-coated slides, dewaxed, and rehydrated. Tissue sections were immersed in antigen retrieval treatment at 100ºC for 10 min in citrate sodium buffer (Sigma-Aldrich) and cooled at 25°C. The sections were then blocked with 2% BSA (Sigma-Aldrich) for 30 min and incubated overnight with the following monoclonal rabbit or mouse anti-human primary antibodies: EGFR (clone EP38Y, Abcam, Cambridge, MA, USA; dilution 1:100), $EGFR^{L858R}$ (clone 43B2, Cell Signaling Technology, Danvers, MA, USA; dilution 1:100), NLRP3 (clone Cryo-2, Adipogen Life Sciences, San Diego, CA, USA; dilution 1:100), and HLA-G (clone 4H84, Santa Cruz Biotechnology; dilution 1:50). The sections were then incubated with HRP-conjugated secondary anti-rabbit, anti-mouse, or anti-goat IgG antibodies, followed by incubation with the polymer for 10 min at 25°C. Finally, the sections were visualized with 3, 3′-diaminobenzidine (Dako, Carpinteria, CA, USA) in accordance with the manufacturer's instructions and counterstained with hematoxylin. Quantification of staining was performed by two pathologists using an optical microscope (Nikon, Eclipse 80i, Tokyo, Japan) at 200 × magnification. In addition, the percentage of total EGFR, $EGFR^{L858R}$, NLRP3, and HLA-G expression was automatically quantified using the PAX-it software, Version 7.4 (Midwest Information Systems, Iowa Avenue, USA). For the mouse tissue sections, 10 random high-power fields were selected and examined on each slide. Positive staining for total EGFR, $EGFR^{L858R}$, NLRP3, and HLA-G was assigned a score ranging from 0 to 3^+ (0, positive staining less than 25% in the section; 1, positive staining between 25 and 50% in the section; 2, positive staining between 50 and 75% in the section; 3, positive staining more than 75% in the section). The total grading score was calculated for each specimen using the following equation: total grading score = (% grading negative × 0) + (% grading 1^+ × 1) + (% grading 2^+ × 2) + (% grading 3^+ × 3). The values range from 0 to a maximum of 300.[66]

Stable overexpression of EGFR variants in FaDu-Luc2 cells

The human OSCC cell line, FaDu-Luc2 (FaDu), was obtained from American Type Culture Collection (ATCC, Manassas, VA, USA) and cultured in EMEM (Thermo Fisher Scientific, Waltham, MA, USA) supplemented with 10% FBS at 37°C in the presence of 5% CO_2. Blasticidin (Invivogen) was added according to

the manufacturer's instructions. Human $EGFR^{WT}$, $EGFR^{19del}$, specific $EGFR^{L858R}$, and $EGFR^{vIII}$ plasmids were obtained from Addgene (Watertown, MA, USA), while the pHAGE-puro empty vector alone was used as an experimental control. In brief, lentivirus production was performed by co-transfection of a plasmid DNA mixture with lentivector plus helper plasmids (pMD2G and psPAX2) into 293T cells using Lipofectamine 3000 (Invitrogen, Carlsbad, CA, USA). To generate stable cell lines, sub-confluent FaDu cells were infected with lentiviral particles in serum- and antibiotic-free Opti-MEM medium in the presence of 10 μg/mL polybrene (Sigma-Aldrich) for 6 h and then cultured in complete EMEM medium for 48 h. After infection, puromycin was added to the cell culture to select resistant cells. The puromycin-resistant gene, which was co-expressed in lentiviral-infected cells, served as a selection marker to indicate successful infection of FaDu cells. Monoclonal cell clones were obtained by serial dilution in 96 wells culture plates of the resistant cells. Most of the selected monoclonal cell clones were stable and exhibited similar performance after at least 20 passages.

Cell viability assay

Cell viability was evaluated *in vitro* using the MTT assay (Sigma-Aldrich). In brief, mock, $EGFR^{WT}$, $EGFR^{19del}$, $EGFR^{L858R}$, and EGFRvIII-overexpressing FaDu cells were seeded in 96-well plates at a density of 6×10^4 cells/mL and allowed to grow for 12, 24, 48, and 72 h. The MTT assay was performed according to the manufacturer's instructions at the indicated time points, including baseline and for each group. MTT reagent (5 mg/mL) was added to the wells followed by incubating for further 4 h at 37°C. The cell culture plate was centrifuged at 1,800 rpm for 10 min at 25°C to remove the supernatant. Afterwards, the formazan crystals were dissolved in 150 μL of DMSO and agitated for 10 min. The amount of MTT-formazan was determined using an ELISA reader at an absorbance of 450 nm.

Transwell migration and scratch wound healing assay

Cell migration was assessed using a Transwell migration assay. In brief, mock, $EGFR^{WT}$, $EGFR^{19del}$, $EGFR^{L858R}$, and $EGFR^{vIII}$ overexpressing FaDu cells were seeded into the top chamber of a 24 well Transwell plate (Corning, Acton, MA, USA) with a porous membrane (8.0 μm pore size) at a density of 2×10^5 cells/mL. Medium supplemented with high serum (20 % FBS) was used as a chemoattractant in the lower chamber. The cells were incubated at 37°C for 24 h. Cells that did not migrate through the pores were removed using a cotton swab and cells on the lower surface of the membrane were stained with crystal violet (Sigma-Aldrich). The number of migrated cells was counted in five randomly selected fields at 100 × magnification using an optical microscope (Nikon). Cell migration was evaluated using the scratch wound healing assay. In brief, mock, $EGFR^{WT}$, $EGFR^{19del}$, $EGFR^{L858R}$, and $EGFR^{vIII}$ overexpressing FaDu cells were treated with the pharmacological inhibitor mitomycin C (Sigma-Aldrich, 10 μg/mL) for 4 h to block cell proliferation. Cells were then seeded in 24 well plates at a density of 5×10^5 cells/mL in serum-free EMEM and cultured overnight prior to initiating the experiment. The confluent cell monolayer was scraped using a pipette tip to generate scratch wounds. The cells were then washed once with PBS to remove dead cells, and the culture medium was re-added to the wells. Subsequently, images were captured using optical microscope (Nikon) to record the wound width at 0 h. Cells were incubated at 37°C for 24 h with the conditioned medium. Images were captured after incubation for 24 h to evaluate cell migration. The wound area was analyzed at each time point of observation based on the mean of five randomly selected fields of view from each scratch using ImageJ software (version 1.46; National Institutes of Health, Bethesda, MD, USA).

Cell invasion assay

The Transwell invasion assay was modified to perform the migration assay. In brief, Matrigel (BD Biosciences) was thawed, added on top of the Transwell membrane and solidified at 37°C for 30 min to form a gel layer. The mock, $EGFR^{WT}$, $EGFR^{19del}$, $EGFR^{L858R}$, and $EGFR^{vIII}$ overexpressed FaDu-Luc2 cells were then added on top of the Matrigel to simulate invasion through the extracellular matrix at 37°C for 24 h. Cells on the top of the membrane were removed using a cotton swab and cells on the lower surface of the membrane were stained with crystal violet (Sigma-Aldrich). Invasive cells were counted in five randomly selected fields at a magnification of 100 × using an optical microscope (Nikon).

ICC

The mock, $EGFR^{WT}$, $EGFR^{19del}$, $EGFR^{L858R}$, and EGFRvIII-overexpressing FaDu cells were seeded on sterile glass coverslips in 12-well plates at a density of 5×10^4 cells/ml overnight 37°C. The culture medium was aspirated, and the cells were washed with PBS at 25°C. The coverslips were then fixed in -20°C methanol for

10 min and incubated in 0.5% Triton X-100 for 5 min. To reduce background fluorescence, coverslips were blocked with 2% BSA prepared in PBS for 1 h. Primary antibodies HLA-G (clone 4H84, Santa Cruz Biotechnology; dilution 1:50) and pan cadherin antibody (GeneTex, Irvine, CA, USA; dilution 1:100) were added to the coverslips overnight at 4°C. The coverslips were then washed in PBS three times for 5 min each and incubated with fluorochrome-conjugated secondary antibodies in 1% BSA for 30 min. The coverslips were then mounted using a fluorescence antifade agent with DAPI (Invitrogen). Images were captured and analyzed using a confocal microscope (Leica TCS SP8 X, Wetzlar, Hesse, Germany).

Expansion of primary T cells

Human T lymphocytes were isolated from peripheral blood mononuclear cells (PBMC) by negative selection kits according to the manufacturer's instructions (STEMCELL Technologies, Vancouver, BC, Canada). T cells were then cultured in RPMI containing 500 IU/mL rhIL-2 (PeproTech, Cranbury, NJ, USA) and anti-human monospecific tetrameric CD3, CD28, and CD2 antibodies (STEMCELL Technologies) at a density of 1×10^6 cells/mL. After 3 days of activation, viable T cells were counted, and the viable cell density was adjusted by adding fresh complete cell expansion medium to the cell suspension. The cells were incubated at 37°C until the desired cell number is obtained.

Transduction of T cells with anti-HLA-G CAR lentiviral practices

Anti-HLA-G scFv fragments were prepared by screening a HuScL-2 human single-chain antibody library (Creative Biolabs, Shirley, NY, USA). Candidate clones from the fourth eluate were selected for ELISA using monoclonal phages after four rounds of panning. Positive clones from phage ELISA experiments were sequenced to obtain the scFv sequence. The clone with the highest affinity was selected as the scFv for constructing anti-HLA-G CAR. The anti-HLA-G CAR insert was constructed by synthesizing DNA corresponding to the leading peptide sequence and was fused to the anti-HLA-G scFv sequence, followed by DNA encoding the transmembrane and cytosolic domains of CD28, IL-2RB, and CD3 zeta. The insert was cloned into the pCAR-(puroless) lentiviral vector (Creative Biolabs) using EcoRI/XbaI restriction enzyme sites. The plasmid contained transmembrane and cytosolic domains, but without the anti-HLA-G scFv sequence as a mock control. The anti-HLA-G CAR plasmid was co-transfected with pMD2G and psPAX2 into 293T cells at a 5:3:1 ratio using Lipofectamine 3000 (Invitrogen), according to the manufacturer's instructions. After 48 h, the virus-containing supernatant was collected for T cell transduction. T cells at a density of 1×10^6 cells/mL were infected with lentiviral particles in serum-free Opti-MEM medium in the presence of 10 μg/mL polybrene (Sigma-Aldrich) overnight. The following day, the virus-containing medium was replaced with complete RPMI medium containing rhIL-2 (PeproTech) for 2 days.

Flow cytometric analysis

The expression of the anti-HLA-G fragment on the cell membrane of T cells was examined using protein L staining (Sigma-Aldrich) as described previously (Hu et al., 2019). Briefly, mock and anti-HLA-G CAR viral particles were transduced into parental T cells. The cells were resuspended in PBS and incubated with protein L (10 μg/mL) containing 4% FBS for 45 min at 25°C. After washing with PBS three times, the cells were incubated with 5 μg/mL of Alexa Fluor 647-conjugated streptavidin (Thermo Fisher Scientific) and FITC-conjugated anti-human CD3 antibody for 1 h. Flow cytometry analysis was performed to examine the protein L-positive cells. Mock T cells were used as background controls. In addition, HLA-G expression on the cell membrane was determined by labeling with a fluorophore-conjugated anti-human specific antibody. In brief, mock, $EGFR^{WT}$, $EGFR^{19del}$, $EGFR^{L858R}$, and $EGFR^{vIII}$ overexpressing FaDu cells were incubated with rhIL-1β (R&D Systems) at the indicated times. Cells were then stained with an anti-HLA-G phycoerythrin antibody (clone 87G, Thermo Fisher Scientific; dilution 1:100) for 1 h at 4°C, the cells were then washed and analyzed using a Cytomics™ FC500 flow cytometer (Beckman Coulter, Brea, CA, USA). The relative expression levels of HLA-G on the cell membrane were determined by comparison with the mean fluorescence intensity of mock control cells.

Cytotoxic killing assay

Cell killing ability was assessed using CellTracker Green (Thermo Fisher Scientific) and PI (BD Biosciences) staining. In brief, mock, $EGFR^{L858R}$ overexpressed, HLA-G overexpressed, and HLA-G knockdown FaDu cells were seeded in 12 well Corning plates at a density of 2×10^5 cells/mL overnight. The cells were then washed and incubated with 1 μg/mL CellTracker Green for 30 min. Subsequently, mock and anti-HLA-G CAR T cells were co-cultured with stained FaDu cells at ratios of 1:1, 3:1, and 6:1 in 1 mL of medium

with IL-2 (100 U/mL) for 24, 48, and 72 h at 37°C. The control groups contained only the target cells. The co-cultured cells were stained with PI to detect cell death. The target cells were determined based on their size and CellTracker green staining, and the presence of granules and PI populations were considered dead cells. Cell killing ability was presented as the percentage of FaDu cell death in the total cell population.

Short hairpin RNA and small interfering RNA delivery

Specific human EGFR, HLA-G, and NLRP3 (Santa Cruz Biotechnology) shRNA and their negative control shRNA were transfected into FaDu cells using Lipofectamine 3000 (Invitrogen) for 48 h according to the manufacturer's protocols. The transfected cells were selected using puromycin (Sigma-Aldrich), and a single cell clone was expanded and harvested to determine the knockdown efficiency by immunoblotting with specific antibodies. The cells were then treated with rhEGF for the indicated times and subjected to other assays.

In parallel, $EGFR^{L858R}$ siRNA was designed to specific target of the nucleotide sequence: 5′-CACAGAT TTTGGGCGGGCCAA-3′ (Qiagen, Valencia, CA, USA). Transfection of siRNAs was performed with Lipofectamine 3000 (Invitrogen) according to the manufacturer's instructions.[67]

Western blotting

Protein was extracted from the cell samples and used for western blot analysis. Briefly, cells were harvested by centrifugation and resuspended in protease inhibitor cocktail-containing PRO-PREP protein extraction buffer (iNtRON Biotechnology, Seongnam-Si, Gyeonggi-do, South Korea). After centrifugation, the supernatants were collected, and protein concentrations were determined using the Bradford protein assay (Thermo Fisher Scientific). Equal amounts of protein samples were separated on SDS-polyacrylamide gels and blotted onto 0.22 μm PVDF membranes (Millipore, Burlington, MA, USA). The membranes were then incubated in blocking buffer (Tris-buffered saline containing 5 % skim milk) for 1 h at 25°C and incubated with primary antibodies against phospho EGFR (Abcam), wild-type EGFR (Abcam), E746-A750del specific EGFR (Cell Signaling Technology), L858R specific EGFR (Cell Signaling Technology), EGFRvIII (Novus Biologicals, Centennial, CO, USA), phospho-p44/42 MAPK (Cell Signaling Technology), p44/42 MAPK (Cell Signaling Technology), phospho-JNK (Cell Signaling Technology), JNK antibody (Cell Signaling Technology), phospho-p38 (Cell Signaling Technology), p38 (Cell Signaling Technology), NLRP3 (Adipogen Life Sciences), human IL-1β (R&D Systems), HLA-G (clone 4H84, Santa Cruz Biotechnology), E-cadherin (GeneTex), vimentin (GeneTex), or β-actin (GeneTex) in 2% skim milk containing TBS with Tween at 4°C. The membranes were then washed and incubated with HRP-conjugated mouse anti-rabbit IgG antibody (Santa Cruz Biotechnology) or HRP-conjugated m-IgGκ BP (Santa Cruz Biotechnology) for 1 h at 25°C. The blots were then immersed in Chemiluminescent Reagent Plus (PerkinElmer Life Sciences, Boston, MA, USA) for 1 min, and chemiluminescence was detected using a ChemiDoc Imaging System (Bio-Rad, Hercules CA, USA). β-actin was used as an internal control.

ELISA

Protein levels of human IL-1β and IL-18 in cell culture supernatants were detected using commercial IL-1β/IL-1F2 Quantikine ELISA Kits (R&D Systems) and human IL-18 ELISA kit (ABclonal, Woburn, MA, USA), respectively, according to the manufacturer's instructions. OD was measured using a multimode ELISA plate reader (BioTek Instruments, Winooski, VT, USA). The supernatant from lipopolysaccharide-stimulated (100 ng/ml, Sigma-Aldrich) PBMC culture served as a positive control for IL-18.[68]

In addition, cell-based ELISA was performed to elucidate which type of HLA-G isoform could be recognized by our anti-HLA-G CAR-T cells. The mock T or anti-HLA-G CAT-T cells were seeded in polylysine-coated 96 well plates at 37 °C for 24 h. After washing, several HLA-G recombinant protein isoforms were added. During detection, HRP conjugation, and chromogenic reaction, the optical density of each well was immediately determined by a microplate reader set to 450 nm. This was followed by evaluation of the cross-reactivity among anti-HLA-G CAR-T cells and HLA-G isoforms.

Study approval

Human cross-sectional study was approved by the Institutional Review Board of CMUH (CMUH108-REC3-041). Written informed consent was obtained from each participant before enrolling in the study. The study was conducted in accordance with the principles of the Declaration of Helsinki. The experimental procedures for *in vivo* studies were approved by the Animal Protection Association of the Republic of China (ROC), and all animal

protocols were approved by the CMU Institutional Animal Care and Utilization Committee (IACUC, CMUIACUC-2018-234). The number of animals used was approved by the ethical committee of the Ministry of Science and Technology (MOST) in Taiwan (MOST 110-2314-B-039-052 and MOST 108-2320-B-039-046). The experiments were performed such that the number of animals used was minimized. We confirm that all methods were performed in accordance with the relevant guidelines and regulations.

QUANTIFICATION AND STATISTICAL ANALYSIS

All independent experiments were performed in triplicate, and all assay conditions were tested in duplicate. In this study, correlations in IHC staining were analyzed using Spearman's correlation test. For *in vitro* studies, data were presented as mean ± SEM and analyzed using one-way ANOVA with a subsequent Scheffe test. For animal experiments, data were presented as mean ± SEM and determined using a paired *t-test*, and the survival rate was analyzed using the Kaplan–Meier estimate and log-rank test. Statistical significance was set at $p < 0.05$.